electricity

MDPI

Article

Enhancing Power Quality in a PV/Wind Smart Grid with Artificial Intelligence Using Inverter Control and Artificial Neural Network Techniques

Musawenkosi Lethumcebo Thanduxolo Zulu *, Rudiren Sarma and Remy Tiako

Discipline of Electrical, Electronic and Computer Engineering, University of KwaZulu-Natal, Durban 4001, KwaZulu-Natal, South Africa; sarmar@ukzn.ac.za (R.S.); tiako@ukzn.ac.za (R.T.)
* Correspondence: 212507083@stu.ukzn.ac.za; Tel.: +27-82-053-9333

Abstract: Power systems need to meet the ever-increasing demand for higher quality and reliability of electricity in distribution systems while remaining sustainable, secure, and economical. The globe is moving toward using renewable energy sources to provide electricity. An evaluation of the influence of artificial intelligence (AI) on the accomplishment of SDG7 (affordable and clean energy) is necessary in light of AI's development and expanding impact across numerous sectors. Microgrids are gaining popularity due to their ability to facilitate distributed energy resources (DERs) and form critical client-centered integrated energy coordination. However, it is a difficult task to integrate, coordinate, and control multiple DERs while also managing the energy transition in this environment. To achieve low operational costs and high reliability, inverter control is critical in distributed generation (DG) microgrids, and the application of artificial neural networks (ANNs) is vital. In this paper, a power management strategy (PMS) based on Inverter Control and Artificial Neural Network (ICANN) technique is proposed for the control of DC–AC microgrids with PV-Wind hybrid systems. The proposed combined control strategy aims to improve power quality enhancement. ensuring access to affordable, reliable, sustainable, and modern energy for all. Additionally, a review of the rising role and application of AI in the use of renewable energy to achieve the SDGs is performed. MATLAB/SIMULINK is used for simulations in this study. The results from the measures of the inverter control, m, VL-L, and Vph_rms, reveal that the power generated from the hybrid microgrid is reliable and its performance is capable of providing power quality enhancement in microgrids through controlling the inverter side of the system. The technique produced satisfactory results and the PV/wind hybrid microgrid system revealed stability and outstanding performance.

Keywords: inverter control (IC); microgrid; droop control; power quality; distributed generators (DGs); artificial intelligence (AI) techniques; PV-wind hybrid; artificial neural network (ANN)

check for updates

Academic Editors: Jose Luis Rueda and Mihaela Popescu

Received: 11 February 2025
Revised: 19 April 2025
Accepted: 27 May 2025
Published: 13 June 2025

Citation: Zulu, M.L.T.; Sarma, R.; Tiako, R. Enhancing Power Quality in a PV/Wind Smart Grid with Artificial Intelligence Using Inverter Control and Artificial Neural Network Techniques. *Electricity* **2025**, *6*, 35. https://doi.org/10.3390/electricity6020035

Copyright: © 2025 by the authors. Licensee MDPI, Basel, Switzerland. This article is an open access article distributed under the terms and conditions of the Creative Commons Attribution (CC BY) license (https://creativecommons.org/licenses/by/4.0/).

1. Introduction

Global warming and environmental challenges, including air pollution, forest loss, ozone depletion, acid rain, greenhouse gases (GHGs), water and land use, species extinction, and radioactive emissions, are all tied to issues with the use and supply of energy [1]. In addition, the existing energy supply affects both the social and economic spheres, leading to several urgent socioeconomic issues [2]. These issues must be resolved collaboratively for people to have an energy future that is optimistic and bright and has fewer negative effects on the environment, the economy, and society. The world is now turning to using

these resources within a certain limit to achieve this goal and combat the traditional energy plants' well-known negative effects on sustainability development (i.e., coal, oil, and natural gas). The focus has been shifted to renewable energy (RE) sources, such as wind, solar photovoltaic (PV), hydropower, geothermal, tidal, and biomass sources [3]. Future network technologies like microgrids have been conceptualized as a result of recent advancements in distributed generation (DG) and electrical power systems. The integration of DERs and other forms of distributed output can be encouraged in small autonomous power system areas, which can also increase stability and efficiency [4]. The use of RE sources helps to achieve environmentally sound technology, low electricity costs, job creation, improved health, and community development, especially in rural areas and developing countries, alongside no or minimal emission production of poisonous and exhaust gases, such as sulfur dioxide, carbon monoxide, and carbon dioxide [5]. As a result, related environmental, economic, and social issues can be reduced. The renewable energy industry will have installed more than 256 GW of capacity by the end of 2020, which will set a record high. The total installed capacity of renewable energy has increased by roughly 10% to 2839 GW globally. In 2020, 139 GW of solar PV installed, 93 GW of installed wind, and 20 GW of installed hydropower. Additionally, 0.1 GW of new geothermal power generating capacity came online in 2020, bringing the global total to about 14.1 GW, as well as 527 MW of ocean power, including tidal capacity [6].

In a related development, artificial intelligence (AI), after years of growth and evolution, has started to significantly influence our daily lives and is beginning to have a significant impact on the disciplines of sustainable growth and development. Accordingly, AI can completely transform the RE industry and is crucial to the substantial rise in RE utilization and contribution to the energy mix [7]. Improved safety and reliability, cost savings, strategies to lessen environmental and climate impacts, increased energy efficiency, market expansion for RE, enhanced integration of microgrids (MG) and smart grid, production of more accurate RE predictions, and optimal operation of RE sources are just a few of the applications and methods for developing RE that use AI [8]. Accordingly, studies in the literature show that the use of AI for RE operation and utilization (AI-based RE) always has a positive influence on RE use, and the negative impact is essentially insignificant. In the long or short term, the use of RE and RE based on AI will be important for sustainability. According to the literature, while RE consumption may have certain negative effects, the prospective effects of RE and AI-based RE positively affect sustainable development [9]. Some recent research looked at the connection between RE and the accomplishment of sustainable development goal 7 (SDG7)'s target (affordable and clean energy) [10]. Through power converters, a variety of DG types, including photovoltaics, fuel cells, and microturbines, connect to the network [11]. The sources are more adaptable in their operation and control than conventional electrical machines and are regarded as interface devices [12]. They do, however, also permit system oscillation brought on by network disorders because of their minuscule physical inertia [13]. A microgrid can operate in a standalone or grid-connected mode. The majority of system dynamics in grid-connected mode are controlled by the primary grid due to the comparatively small size of the microsources. In standalone mode, the device's dynamics are mostly dependent on the network itself, micro sources, and power regulation [4,14]. The operational capability of the island is a key distinguishing factor of microgrids. In general, microgrids may support a load cluster if the DG is operational following a disturbance and protection and reconnection issues are properly handled [15]. Currently, the utilization of distributed energy resources (DERs) is growing in reputation and has received significant attention as a practical way to accommodate the rising amount of electricity being consumed. Using a DC microgrid is a cost-effective way because of their efficacious yet environmentally friendly nature. A microgrid is a type of

electricity system that consists of utilizing one or more groups of renewable energy sources incorporating the energy storage apparatus. Microgrids describe how a distributed power supply is set up in a specific location to meet local load requirements or to connect to the conventional grid. Through the distribution network, the microgrid can be used in tandem with the large-scale power grid and can also independently meet the energy needs of local loads, increasing the dependability of the power supply on the side of the loads [4]. The control procedure is rather straightforward once the microgrid system is connected to the grid. Only the PCC's voltage, amplitude, and phase are managed in synchronization with the grid [5]. The loads have access to both the grid and the microgrid for their electric supply. Only the microgrid can supply the loads with electricity when the microgrid system is operating off-grid. P/Q control, V/F control, and droop control are among the control methods that can be used to efficiently and steadily manage the amplitude and phase of the PCC output voltage [16]. In contrast to other emerging energy sources, photovoltaic and wind power generation has quickly developed and exhibits great reliability, stability, and only minor power fluctuations. It can serve as the best power source for a microgrid. In this study, the micro-voltage grid's source is a series of parallel PV-wind standalones connected to inverter. To share the essential real and reactive powers with other DGs, the inverter includes an outside power loop-based. Figure 1 shows a hybrid PV and wind energy system microgrid, which is a block diagram modeled and presented in this paper.

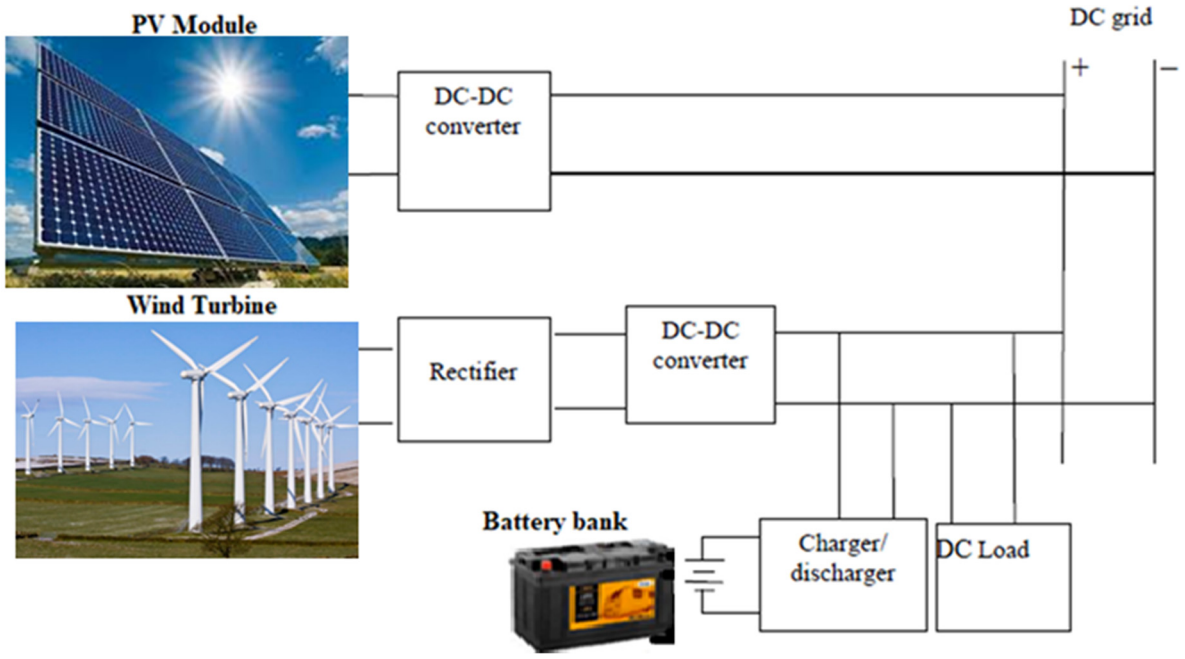


Figure 1. PV-wind hybrid DC microgrid system.

According to the International Energy Agency (IEA), the demand for all other fuels decreased in 2020, while the usage of RE increased by 3%. The main factor was an increase of about 7% in the amount of electricity produced from renewable sources. As a result, the proportion of renewable energy sources in the world's electricity generation increased from 27% in 2019 to 29% in 2020. While the use of bioenergy in industry increased by 3%, the fall in the use of biofuels due to decreasing oil demand largely countered the increase. The biggest annual growth rate since the 1970s is anticipated for renewable electricity generation in 2021, which will increase by more than 8%. Two-thirds of the growth in renewable energy is expected to come from solar PV and wind energy [17].

This paper presents a methodical way to simulate an inverter-based microgrid and apply the artificial neural network (ANN) technique. The extent to which RE use and

AI-based-RE could influence all aspects of sustainable development, as outlined by this research, has not been extensively studied in any prior research publication. This contribution to the study aims to build on the research work reported by investigating the performance of an ANN-based IC in a hybrid PV-wind system under various operating conditions and power analysis. This paper presents the use of artificial intelligence techniques to optimize and improve power quality in an MPPT-based system. In this paper, an enhanced inverter control (IC) and artificial neural network (ANN), combined as the ICANN technique, is used for optimizing and improving power quality in a microgrid system based on MPPT is presented. To increase the RE and AI combination with inverter control for power quality enhancement, performance effectiveness, and efficiency, the ICANN technique has been applied. ANN includes a self-learning capability that makes it simple to adapt the algorithm to various grid disturbances and operational conditions and attain optimal scheduling and management in a hybrid microgrid. The objective function included production control, operation, and power generation. To maximize the energy produced by wind turbines (WTs) and photovoltaic cells (PVs), the ANN is incorporated with inverter control (IC). Additionally, the energy delivered by and stored in the storage system was optimized. The authors of [18] escribed a data-driven fault location method based on fault voltage and current discrepancies in AC/DC microgrids.

To increase the combination of RE and AI with inverter control for power quality enhancement, performance effectiveness, and efficiency, the ICANN technique has been applied.

This article contains the following sections:

Section 2 presents a review of DC-AC microgrid control strategies.

Section 3 presents the application of the inverter control (IC) technique for power quality enhancement, and a summary of the proposed system is highlighted.

Section 4 presents the application of the artificial neural network (ANN) technique for power quality enhancement.

Section 5 provides validation, analysis, and discussion of the simulation and results.

Section 6 delivers the conclusion of this paper, recommendations, and future outlook.

2. DC-AC Microgrid Control Strategies

Renewable energy sources are connected in the form of AC and DC MGs to maximize their efficiency. Both renewable and non-renewable energy sources can be used to power the AC MGs. They enhance the effectiveness and dependability of the current power system architecture and are used in a variety of applications, including those in remote locations, commercial buildings, and as backups for the delivery of electricity. Through power electronic inverters, distributed energy sources and energy storage systems are interfaced with MGs. A crucial component in maintaining the efficient operation of MGs is through the control systems of the power electronic inverters. Hierarchical control serves as the foundation for categorizing control strategies. The many MG control strategies are divided into four different categories: (1) The converter output control, which is in charge of regulating power flow and output current. As a result, the converter output control system may be divided into two groups: the internal control loop (current controller) and external control loop; (2) the power-sharing control, which manages the distribution of power across several parallel converters; and (3) the MG supervisory (secondary) control, which deals with parameter restrictions internal to the MG and provides low levels set points. This is a category for power-sharing approaches based on how dependent they are on communication lines. These control techniques can be divided into two groups: centralized control, which relies on communication lines to transfer control commands from MG supervisory control to lower level controllers, and decentralized control, which

uses local parameters and (4) the grid supervisory (tertiary), which oversees the power transfer between the MG and the main grid [19].

2.1. PV Microgrid Modelling

PV systems make a key contribution to frequency and voltage control in microgrids. Conventionally, power delivery to a utility grid has been the goal of the converters for PV systems. They are a great form of grid-connected current source [18]. Nevertheless, as the use of PV generation spreads, a lack of frequency response and control capabilities could lead to significant frequency swings under loads or solar irradiation difficulties. Because of this, there is an increasing operational need for PV systems to be employed in microgrid frequency and voltage management. Through the use of current sources or voltage sources, PV systems can take part in the frequency and voltage regulation of the microgrid. In response to the issue of the state of charge (SoC) of energy storage systems (ESS) rising above the safe upper limit, authors in [20] introduced an active power controller to reduce the PV power. Since PV converters are managed as current sources, the method in [20] does not, however, permit PV systems to operate independently in autonomous mode. The direct participation of PV converters in frequency regulation has been proposed in [21–23] using voltage-source PV droop techniques. The MPPT function and droop control are switched during load transients using a hybrid PV controller. However, the hybrid control system, which alternates between various configurations, considerably affects the PV system's stability and dependability. Additionally, when many PV systems with ratings in the range of a few kW are used in residential microgrids, two-stage converters are an expensive option and result in significant power loss. For single-stage PV inverters, the use of a universal PV droop controller has recently been discussed [23]. The stability of the microgrid clusters, as will be shown in this research, will be put to the test while employing the suggested PV droop controller.

A photovoltaic effect is used by photovoltaic cells to convert sunlight into voltage. When a load is connected across a PV array, the PV array will supply electricity to the load while drawing current from the device [24]. To create current flow in an external circuit, n-type and p-type materials are used in the building of the PV array. Photons are absorbed by PV cells as a result of the light's collision with the material. A single cell can only provide a voltage between 0.5 and 0.8 volts, which is insufficient to power the load. To enhance the voltage and current, several cells are linked in series and parallel, respectively, as shown in Figures 2 and 3.

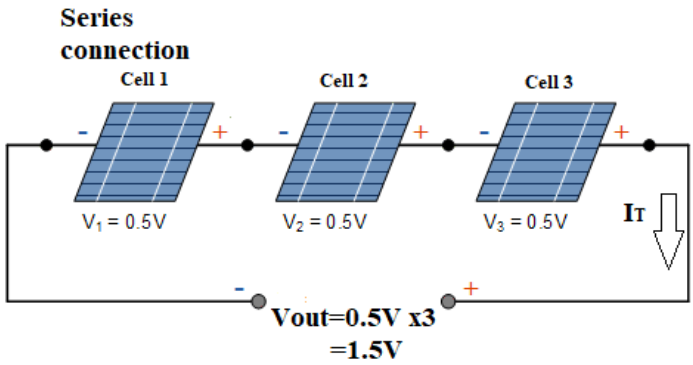


Figure 2. PV voltage increment in series connection.

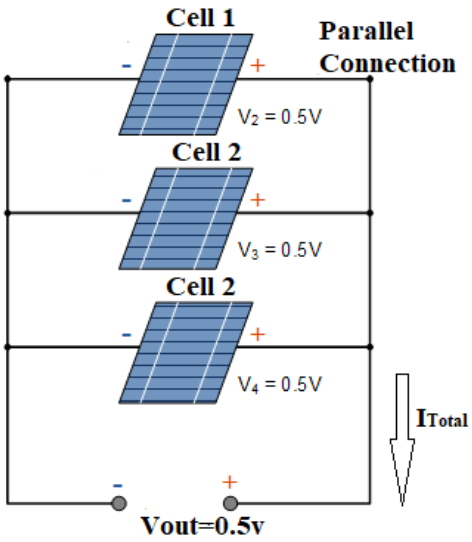


Figure 3. PV current increment in parallel connection.

The most fundamental configuration of any PV system is solar cells. The optimal cell configuration is also taken into account as a current source, where the current from the solar cells is connected to the solar radiation intensity [25,26]. Figure 4 displays solar cells as they are represented in an electrical circuit. Equation (1) represents the current in the solar PV system as follows:

$$I = I_{SC} - I_d - \frac{V}{R_p} \tag{1}$$

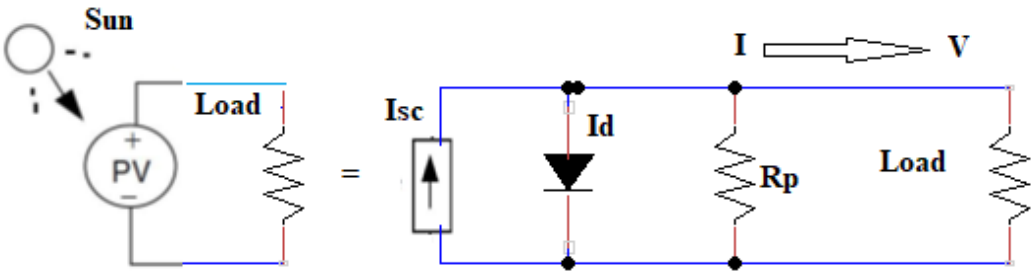


Figure 4. Equivalent circuit of the solar cell with the load connected.

Figure 4 shows a straightforward circuit for a solar cell that can produce electricity, with a real diode running in parallel with a perfect current source. The supplied current varies in direct proportion to the solar cell's flux of direct sunlight [27]. The genuine PV cell's current-voltage characteristic curve is shown in Equation (2):

$$I = I_{SC} - I_o\left(e^{q\left(\frac{V+IR_S}{AKT}\right)} - 1\right) - \left(\frac{V + IR_S}{R_P}\right) \tag{2}$$

where I is the cell current (the same as the module current) (A), I_{SC} is the short circuit current which is equal to photocurrent (A), I_o is the dark saturation current (A), I_d is the diode current, q is an electronic charge ($1.602 \times 10 - 19$C), K is Boltzmann's constant ($1.381 \times 10 - 23$ J/K), A is the idealizing factor, T is cell temperature (K), V is the cell voltage (V), R_S is the shunt resistance (Ω), and R_P is the parallel resistance (Ω).

Retaining the sign convention shown in Figure 4 and relating Kirchhoff's Current Law to the node above the diode, using Equation (3), one can presume that:

$$I_{SC} = I + Id + Ip \tag{3}$$

where Id is a diode current (A) and Ip is a parallel resistance current (A). Rearranging and substituting the Shockley diode equation into Equation (3) at 25 °C, one obtains Equation (4):

$$I = I_{SC} - I_O\left(e^{38.9Vd} - 1\right) - \left(\frac{Vd}{Rp}\right) \tag{4}$$

where Vd is the diode voltage (V). With an assumed value of temperature in a spreadsheet, the current I can be found in Equation (4). The voltage across an individual cell can be found in Equation (5):

$$I = Vd - IRs \tag{5}$$

2.2. Wind Energy Microgrid Modelling

It is possible to use wind energy to power an electrical generator, meaning that wind turbines can generate electricity. As it passes over the blades, the wind produces lift and applies a turning force. The shaft inside the nacelle, which is attached to the generator, is rotated by blades. Synchronous and induction generators can both be used in wind turbine systems [28]. However, because it performs better than other wind turbine generators, a gearless approach is mostly employed in variable-speed multi-pole permanent magnet synchronous generators (PMSG). Since it can operate in a wide range of wind speeds, the variable speed multi-pole permanent magnet makes PMSG the most efficient and dependable system [29]. The PSMG is used in this study because it performs better than other wind turbine types. The continual accessibility of the wind energy source is one additional climate factor that is considered.

Energy generated by a wind turbine, E_w, and the rated output power, P_w, is given by the use of Equations (6) and (7) as follows:

$$P_w = \frac{1}{2}\rho_w A v^3 C_p \mu_g \mu_t \tag{6}$$

$$E_w = E_w \times T \tag{7}$$

where E_w is the energy generated by the wind turbine, P_w is the output power, ρ_w is the density of air in Kg/m^3, A is a swept area of rotor blades, C_p is the power coefficient representing generator and turbine efficiency, μ_g is generator efficiency, and μ_t is turbine efficiency.

The power coefficient can be expressed by the following Equation (8):

$$C_p = \frac{1}{2}\left(\delta - 0.022\beta^2 - 5.6\right)e^{-0.17\delta} \tag{8}$$

where β is the pitch angle of blades in degrees and δ is the tip speed ratio of turbines.

The inertia and the damper are used to model the high-speed shaft. Figure 5 illustrates the combined inertia of the high-speed shaft, generator rotor, and gearbox as well as the friction of the high-speed shaft bearings, aerodynamic torque, generator torque, and gear ratio. Figure 5 also highlights how the wind turbine system, which primarily consists of blades, the gear train, and the generator, is defined using a two-mass model system.

The shaft torque T_{S1}, which is created by the torsional rotation of the low-speed shaft, balances off the turbine torque Tm, which is produced by the wind and increases the inertia of the turbine. The following expression in Equation (9) serves as its representation:

$$T_m - T_{s1} = J_m \frac{\partial \omega b}{\partial t} \tag{9}$$

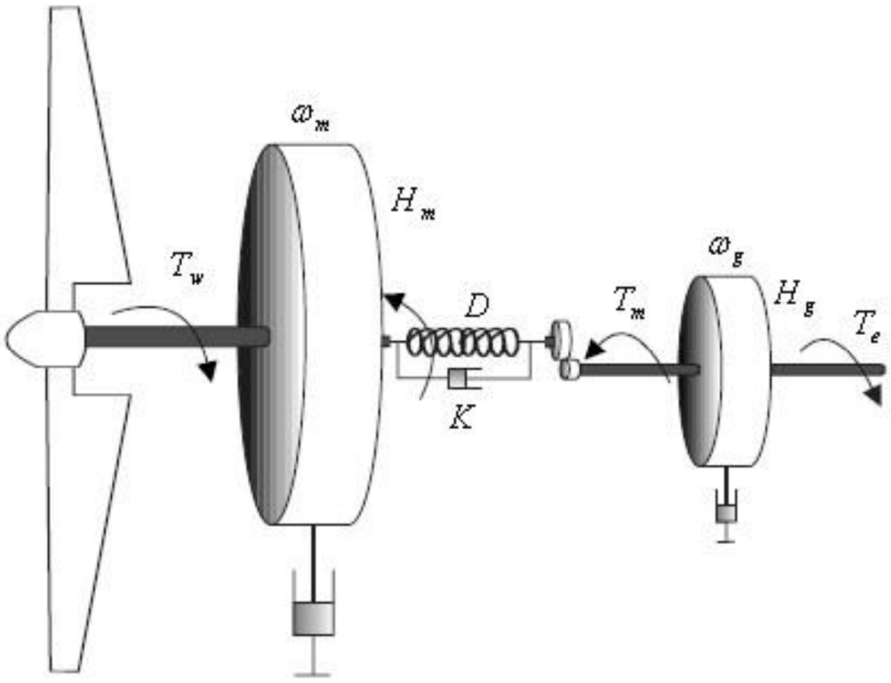


Figure 5. Two-mass model wind turbine [30].

2.3. PV-Wind Hybrid Systems

Large PV plants made up of several panels installed on a sizable ground surface have grown in size and capability. The use of solar energy systems allows for the conversion of solar energy into electrical power. In a photovoltaic (PV) solar system, sunlight is used to illuminate the panels, which then undergo a conversion to produce direct current (DC) electricity. Wind energy conversion is the process of converting the kinetic energy of the wind into electrical energy using wind turbines connected to generators. The lift produced by the wind as it moves over the turbine blades acts as a turning force. This causes the shaft inside the nacelle, which is connected to the generator, and the turbine blades to rotate. Utilizing two renewable energy sources, solar PV and wind energy, in combination with battery storage provides a better and more reliable power supply, making it both more cost-effective and a reliable source of renewable energy to power the load [11]. Different renewable energy sources, storage, and conventional sources are all combined in hybrid power systems. Photovoltaic panels and a wind turbine generator form the suggested system in this research. Through the use of a DC/DC converter for the PV system and an AC/DC converter for the wind system, the two sources are connected to the DC bus. The AC loads are supplied through an inverter. To meet the demand for official buildings, a methodology for the design optimization of PV/wind hybrid systems is supplied. This work identifies the dynamic optimization method and the mathematical model of the hybrid system under study. By considering three design objectives, including economic, reliability index, and environmental profit obtained by using a PV-wind system, the multi-index approach is used to tackle the hybrid system design issue. The suggested optimization strategy is based on a dynamic evaluation of the wind and solar energy needed to serve the appropriate government buildings. Designers can create an exact plan thanks to this dynamic consideration. On the other hand, the multi-index design offers a useful means of acquiring design targets with various preferences.

2.4. Review for Microgrid Control Strategies

Instead of using small-signal models in [31], the authors used a particle swarm optimization (PSO) algorithm that was applied directly to a power-electronic-switch-level

microgrid simulation model for optimization. To account for the system's nonlinearity, optimization was carried out under various operating situations, and the results were satisfactory. However, it is challenging to examine the effects of specific control parameters on overall performance because the control parameters were adjusted collectively independent of levels or types of controllers. In this paper, breaking down the controller design process into modular components is suggested, as well as performing incremental parameter tuning. Three control modes, high, medium, and low frequency, are used in microgrid control, according to reference [12]. Three basic approaches have been established in the study of distributed control theory [32,33]: Cooperative Control, which is based on the consensus theory (or synchronization) of a multi-agent system (MAS) with specified dynamics [34]; Both (Intelligent) Agent Control, which consists of autonomous local agents that perform control actions based on local goals and information from neighbors and the environment, usually utilizing machine-learning techniques [35–37]; and Distributed Optimization, also known as a component of decomposition-based techniques, which shares information between units to solve local optimization problems [38]. An overview of recent research on distributed control systems used with DC-MGs is discussed in [28]. The authors specifically go over asymptotic and finite-time consensus procedures. Problems with communication are also discussed, along with remedies. To accomplish economical electrical energy dispatch in MGs, distributed control techniques are hardly covered in [28], which does not analyze stability. In [29,39], a review of control techniques used with hybrid AC/DCMGs is offered. The secondary control is outside of the scope of the writers in [40], and distributed control approaches are not considered in this article. Instead, the authors in [40] only discuss power management strategies for this form of MG. An overview of small-signal stability techniques for the AC distribution grid that use impedance-based models and are implemented in a synchronous reference frame is presented in [41]. Different stability methods in the temporal domain are compared and analyzed. A review of the small-signal stability of MGs is examined in [42] on the same topic. Incorporating renewable energy into the energy system has emerged as a worldwide priority. As a result, the potential for renewable energy is not spread evenly and is irregular [43]. Furthermore, the best sites for RES are frequently already occupied, and there are limited development opportunities [44], as in Switzerland, where there are valuable natural regions [44,45]. To get around these issues, hybrid systems that mix several renewable energy sources (RES) that work well together and can share power generation infrastructure (such as cable pooling) can be used [46]. In general, RES interaction with thermal power is one of these systems, as are wind–solar coupling and wind–solar–hydro connection [47]. Although cable pooling has many unquestionable benefits (such as easier coordination and optimization of the operation of multiple RES or space savings), its drawback may be a lack of grid connection capacity when excess electricity is produced (for example, in windy and sunny weather), making it challenging to utilize [40].

2.5. Mathematical Model for Controlling Inverter

The contribution to a PI controller whose output determines the actual reference I* injected is given in Equation (10). A proportional-integral controller is used to implement this control, and the controller output is stated in Equation (11).

$$\begin{aligned} {i_d}^* &= \left(k_{pv} + \tfrac{k_{iv}}{s}\right)\left[{v^*}_d - v_d\right] \\ {i_q}^* &= \left(k_{pv} + \tfrac{k_{iv}}{s}\right)\left[{v^*}_d - v_q\right] \end{aligned} \tag{10}$$

$$\begin{aligned} u_d &= \left(k_{pi} + \tfrac{k_{ii}}{s}\right)\left[i^*d - i_d\right] + v_d + (\omega L)i^*q \\ u_q &= \left(k_{pi} + \tfrac{k_{ii}}{s}\right)\left[i^*\mathrm{q} - i_q\right] + v_q - (\omega L)i^*d \end{aligned} \tag{11}$$

where k_{iv} and k_{pv} are the integral gain and proportional gain of the voltage proportional-integral control, respectively, representing the difference between the specified reference and the calculated voltage in the inner loop. The internal current loop nevertheless regulates the output current of the inverter and keeps track of the external voltage loop reference current. Additionally, the current control loop creates the reference voltage (u_d and u_q) of direct-quadrature axes for the PWM in accordance with the current references, i^*_d and i^*_q, generated by the power control loop and voltage control loop in the two systems. The microgrid operating parameters are dynamically changed to suit current conditions by implementing virtual impedance and droop controllers simultaneously. A PI control scheme can also be used to implement the outer voltage controller, with the result of the controller output provided by Equation (12):

$$\begin{aligned} i_d{}^* &= \left(k_{pv} + \frac{k_{iv}}{s}\right)\left[v^*_d - v_d - v_{dpd}\right] \\ i_q{}^* &= \left(k_{pv} + \frac{k_{iv}}{s}\right)\left[v^*_d - v_q - v_{dpq}\right] \end{aligned} \tag{12}$$

where k_{iv} and k_{pv} are the voltage proportional-integral control's integral gain and proportional gain, respectively. The virtual impedance or grid causes a voltage drop known as the v_{dp}.

2.6. Implementation of Inverter Tuning Control Approach

Microgrids provide electricity to nearby loads directly through off-grid control, acting as a voltage source, or even collaborating with an energy storage system. They enhance not only the stability of the loads' power supply but also their economic efficiency [11]. Small-signal stability is one of the major issues with a microgrid's dependable operation. Stability analysis in conventional power systems is widely established, and for the many frequency ranges (or time horizons) of potential concern, some models have the necessary features. Figure 6 shows the PWM IGBT inverter connecting control of an inverter and LC filter modeled in MATLAB (2023a). This paper aims to perform power quality enhancement using an inverter control approach with AI capabilities.

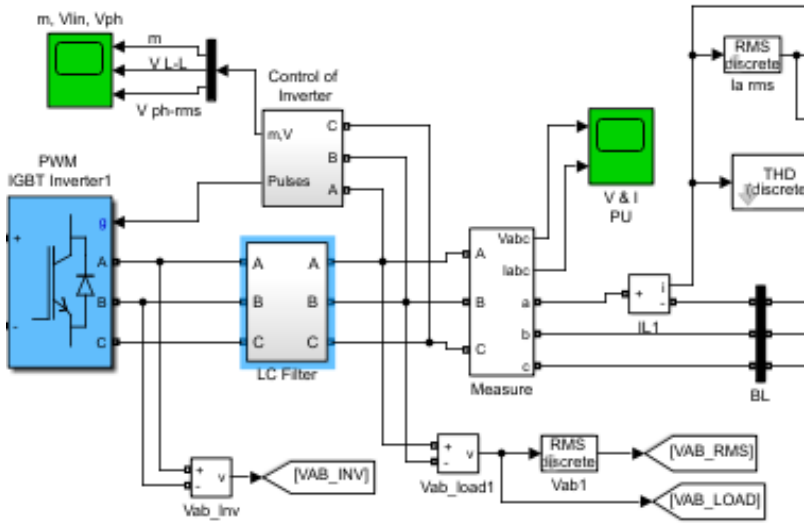


Figure 6. Inverter in a DC/AC microgrid.

3. Application of Inverter Control (IC) Technique for Power Quality Enhancement

The system circuit that was created is shown in Figure 7. This circuit entails distribution generation, which consists of PV-wind connected to CC-VSI for interface with the grid via

a DC-link capacitor that stores energy [48]. The highest power from the PV and wind is retrieved using the extended search algorithm. A reference DC link voltage is generated; then, the IGBT inverter is used to produce AC. When there is no solar energy, the reference DC-link voltage is set to its default value [49]. The AC side of the VSI is connected to an inductive filter. Before the system is connected to PCC, a step-up transformer is used to raise the voltage level. The PCC is coupled to a non-linear uncontrolled rectifier load [50,51]. An inverter control is utilized to reduce the load current harmonics and power factor and control the flow of DG power to the PCC [48].

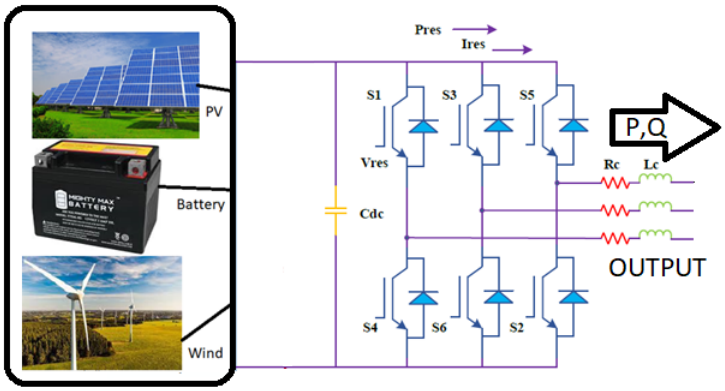


Figure 7. Voltage source inverter.

3.1. Control of the Inverter

The power from the DC microgrid is then changed to AC using converters. To enhance quality power, the inverter parameters are tuned to produce power that meets the demands. Figure 8 shows the control of the inverter circuit, with Vph, VL-L, and Vph_rms as output measured results in this research. The Vph is connected to a discrete PWM generator through Vabc_inverter, with two pulses generated per the designed equation.

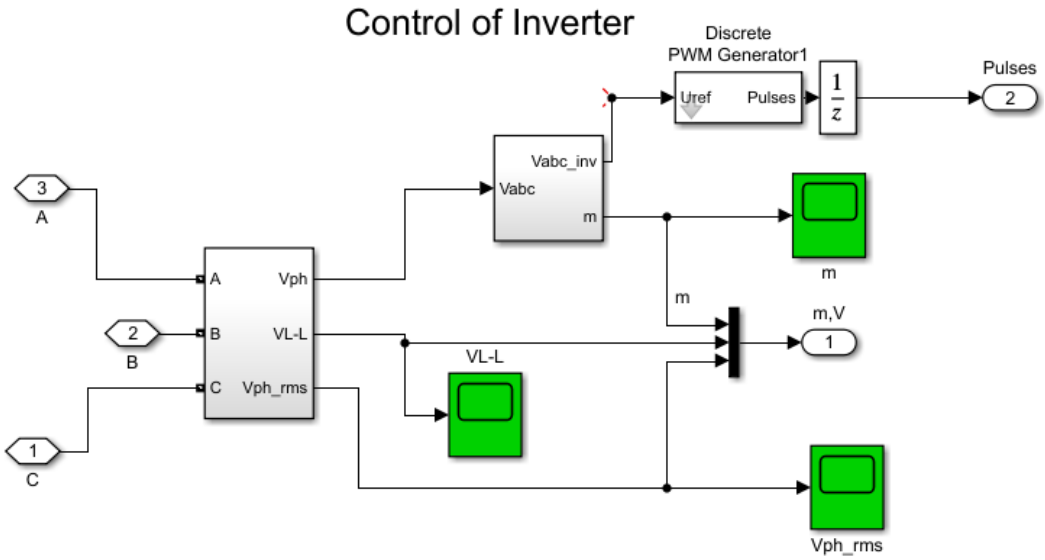


Figure 8. Control of inverter circuit.

3.2. Control of the Inverter

LC Filter Connection. While the inner loop controls the current set via the inverter-based microgrid, the outer loop regulates the voltage to meet its reference value. To keep the output voltage close to the voltage control loop connection, the capacitor C is charged by the controlled voltage. The output filter plays a crucial role in the grid-connected inverter's

ability to filter high-frequency switching harmonics. Input filters like the basic LC are frequently used in grid-connector applications to reduce current harmonics. The typical LC filter must have a high filter inductance to meet the requirements for current harmonics, which raises the filter's size and price. By reducing the current harmonics coming from the grid-tied inverter (GTI), the LC filter eliminates the issue. The internal part of a filter and its voltage measurement connection are shown in Figure 9.

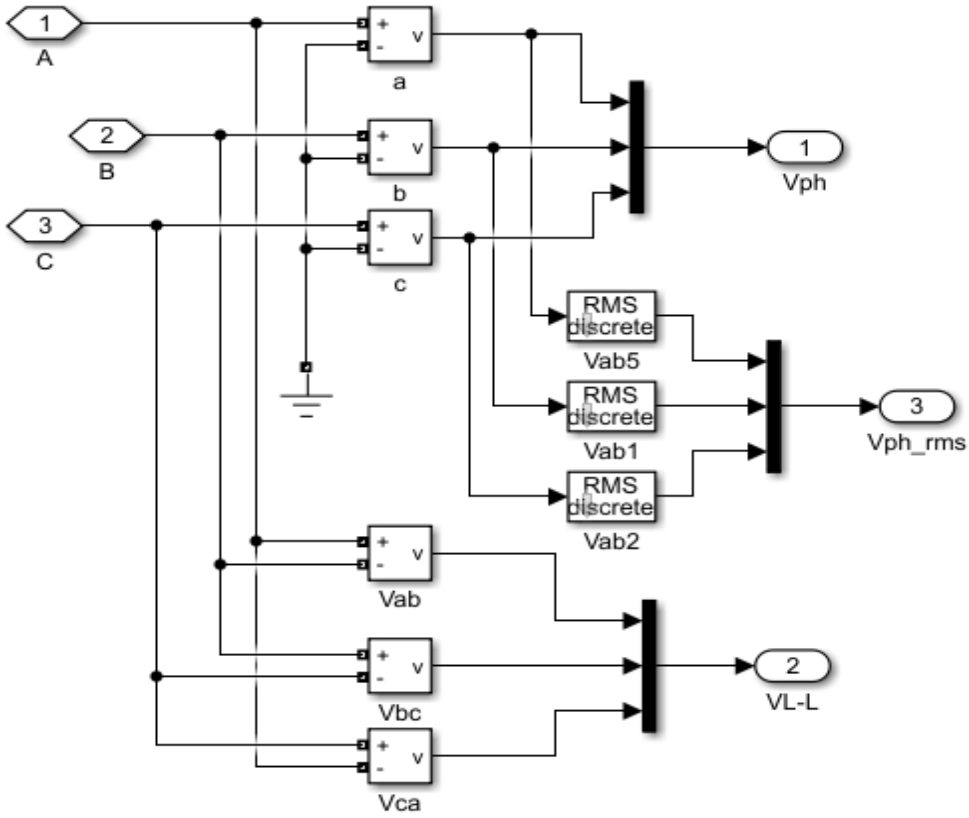


Figure 9. Voltage measurements filter circuit.

4. Application of Artificial Neural Network (ANN) Technique for Power Quality Enhancement

A highly computational model known as an artificial neural network (ANN) can be adjusted to learn input-to-output mappings based on prior data. Figure 10 illustrates the three layers that make up an ANN: the input layer, the hidden levels (computational layers), and the output layer. In ANN, feed-forward propagation and back-propagation are where the computation weight and bias take place. Back-propagation reduces the error between the real and estimated outcomes, but feed-forward propagation accurately estimates the results. The neural network's input dataset was processed in the input layer. Figure 10 illustrates how (xi) displays the data provided as an ANN input at the beginning of an ANN training process. Each hidden layer of the ANN multiplies the input data by weights and adds it to the bias. The accuracy of the ANN-derived prediction rises with the number of hidden layers. The output layer combines the data from the hidden levels to produce the required result for the program in consideration.

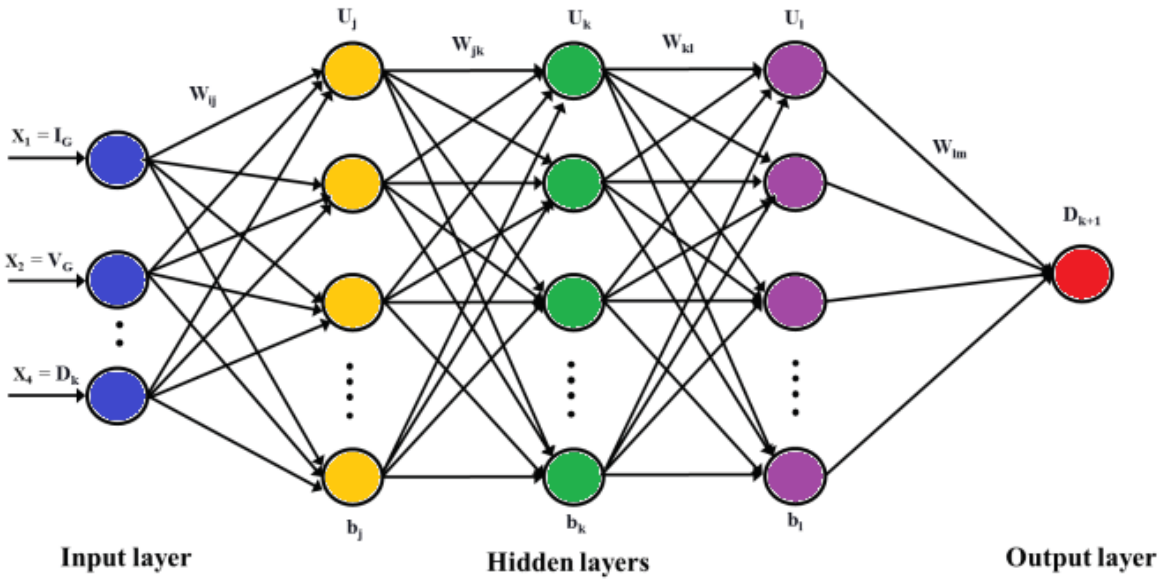


Figure 10. Basic arrangement of ANN.

4.1. Review for ANN Control Strategies in Microgrids

In [52], a multi-agent ML model for AC microgrid protection in both grid-tied and islanded modes was constructed. The ANN algorithm was used to categorize a specific fault after the machine learning (ML) model has been trained using the collected fault data. When a fault occurs, many agents begin talking to coordinate and segregate the issue. The suggested effort can offer both main and backup protection in grid-connected and self-contained microgrids, according to the results. Table 1 presents the results for AC microgrids and provides an overview of AI-based primary and secondary control approaches. The findings are summarized in the table based on several other crucial factors. The two main architecture types are centralized and distributed. Only one of the ANN-based solutions has been validated in a real-time experiment, and the others have mostly been practiced. Similar to DC microgrids, AC microgrids are primarily explored in off-grid situations. To integrate AI in islanding detection and reconnection mechanisms, grid-connected situations should be the main focus.

Table 1. AI-based primary and secondary control in AC microgrids.

Ref.	AI Technique	Control Strategy	Objectives	Grid Connect (On/Off/Both)
[53]	ANN	Centralized	Voltage and frequency regulation	Off
[54]	ANN	Centralized	Frequency regulation	Off
[55]	ANFIS	Centralized	Reactive Power Sharing	Off
[56]	ANN	Distributed	Voltage and frequency regulation	Off
[57]	ANN	Distributed	Frequency regulation	Off
[58]	ANN	Distributed	Voltage and frequency regulation	Off
[59]	ANN	Not specified	Optimal control	On
[60]	ANN	Not specified	Power quality control	On

4.2. Adoption for ANN in PV-Wind Hybrid Systems

Tertiary control, which functions in relation to the tasks connected to the distribution/at the networked level, is the top layer in the hierarchical control scheme. The tertiary layer controls both the best possible power flow within microgrid units and the import/export of power from the external grid. To ensure efficient and effective power dispatch from each DER unit while minimizing operational costs, coordination is therefore a crucial control layer [61]. The DER units are also permitted to engage in the energy market and offer grid support services to other nearby microgrids and external grids through the inclusion of energy market-related operations under this supervision. The use of AI-based methodologies can hasten research into solutions to control difficulties related to this layer. The gradient descent algorithm involves phases of (i) determining the gradient of the loss/error function and (ii) updating the current parameters in response to the system fluctuation. This procedure is repeated until the cost function's minimum is reached [62].

4.3. Mathematical Model for Controlling ANN in a PV-Wind Hybrid Systems

4.3.1. Gradient Descent

Finding a local minimum of a differentiable function that significantly reduces a cost function is achieved using the optimization process known as gradient descent. When the inputs are slightly altered, a gradient adjusts the weights and measures the variation in the output. Equation (13) describes the cost function used to lessen the discrepancy between the predicted and the ideal result:

$$f(w,\ b) = \frac{1}{N}\sum_{i=1}^{n}(y_i - (wx_i + b))^2 \tag{13}$$

Therefore, Equation (13) can be used to find the gradient of the cost function as in Equation (14):

$$f'(w,\ b) = \begin{pmatrix} \frac{df}{dw} \\ \frac{df}{db} \end{pmatrix} = \begin{pmatrix} \frac{1}{N}\sum -2x_i(y_i - (wx_i + b)) \\ \frac{1}{N}\sum -2(y_i - (wx_i + b)) \end{pmatrix} \tag{14}$$

The hidden layer's new weights 'w' and biases 'b' are determined by iterating over the input datasets. The gradient function is then solved by computing the partial derivatives. The direction in which we can move our parameters to minimize the cost function is indicated by this new gradient, which also shows the slope of our cost function at our current position (the current parameter values). A hyper-parameter for lowering the cost function is the learning rate. When an ANN is being trained, this learning rate acts as a hyper-parameter to control the size of our update (α = 0.001). To produce the required result, the model is trained for 100 epochs.

4.3.2. Derivative of Sigmoid Function

The PWM signal delivered to the switch of GTI (0/1) is the intended output from the ANN controller. The sigmoid activation function, which has a probability range of 0 to 1, is utilized as an activation function to restrict the output values sent to GTI switches as given in Equation (15). The sigmoid function gives 0.5 as a result when the input is 0. It returns a value that is quite close to 1 if the input is a significant positive number. The sigmoid function returns a value that is very near to zero when a negative number is supplied. It is useful in models where the result must be projected as an output because of this.

$$f(x) = \frac{1}{1 + e^{-x}} \tag{15}$$

4.3.3. Application and Modelling of ICANN in PV-Wind Hybrid Systems

The focus of this paper is microgrid applications of cooperative and distributed control systems based on the application of the artificial intelligence technique ANN in combination with the inverter control (IC) approach. Because of simplicity, the generic name of Distributed Control is used in the rest of this work. Regarding cooperative control, asymptotic consensus protocols are the defining element for cooperation in ICANN. They are also the basis on which other techniques and improvements for convergence speed and stability are being deliberated. An artificial neural network works by multiplying weights and adding bias in a pipeline scenario at the intermediate level; the network's main function maps any input to the desired goal value. The parameters (weights of the hidden layer) that minimize the cost function and reduce the difference between the predicted value and the model output are determined by training the artificial neural network with the existing dataset. The ICANN technique applied is shown in Figure 11, a PV/wind system with energy storage is modeled and simulated on MATLAB/Simulink, and the AC loads are connected to the system.

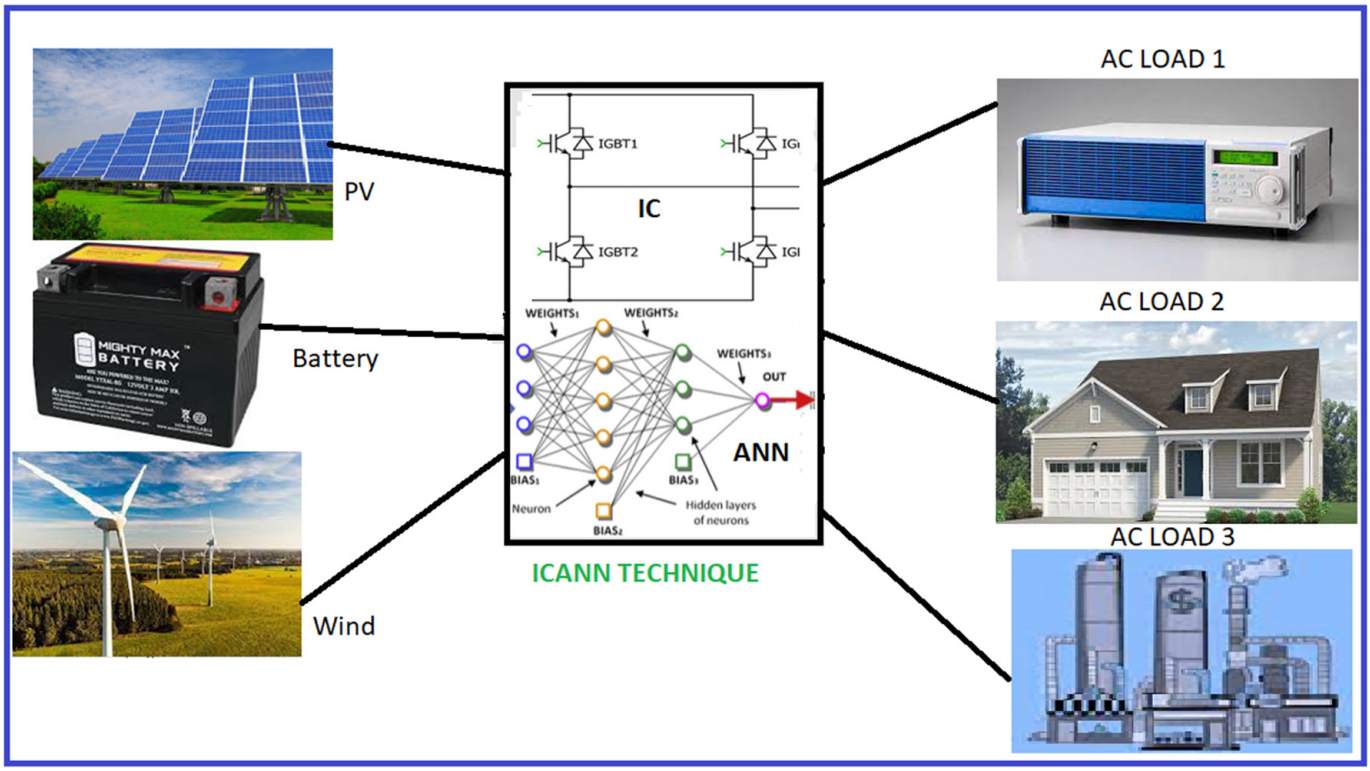


Figure 11. Main ICANN technique application control block.

5. Simulation and Results

Although the analysis of the standalone microgrid's steadiness of traditional power systems is well established, it is necessary to determine how circuit and management elements contribute to specific oscillatory modes and which of these have reduced damping in inverter-based microgrids. Figure 12 shows a PV-wind hybrid microgrid system input DC side in MATLAB/Simulink.

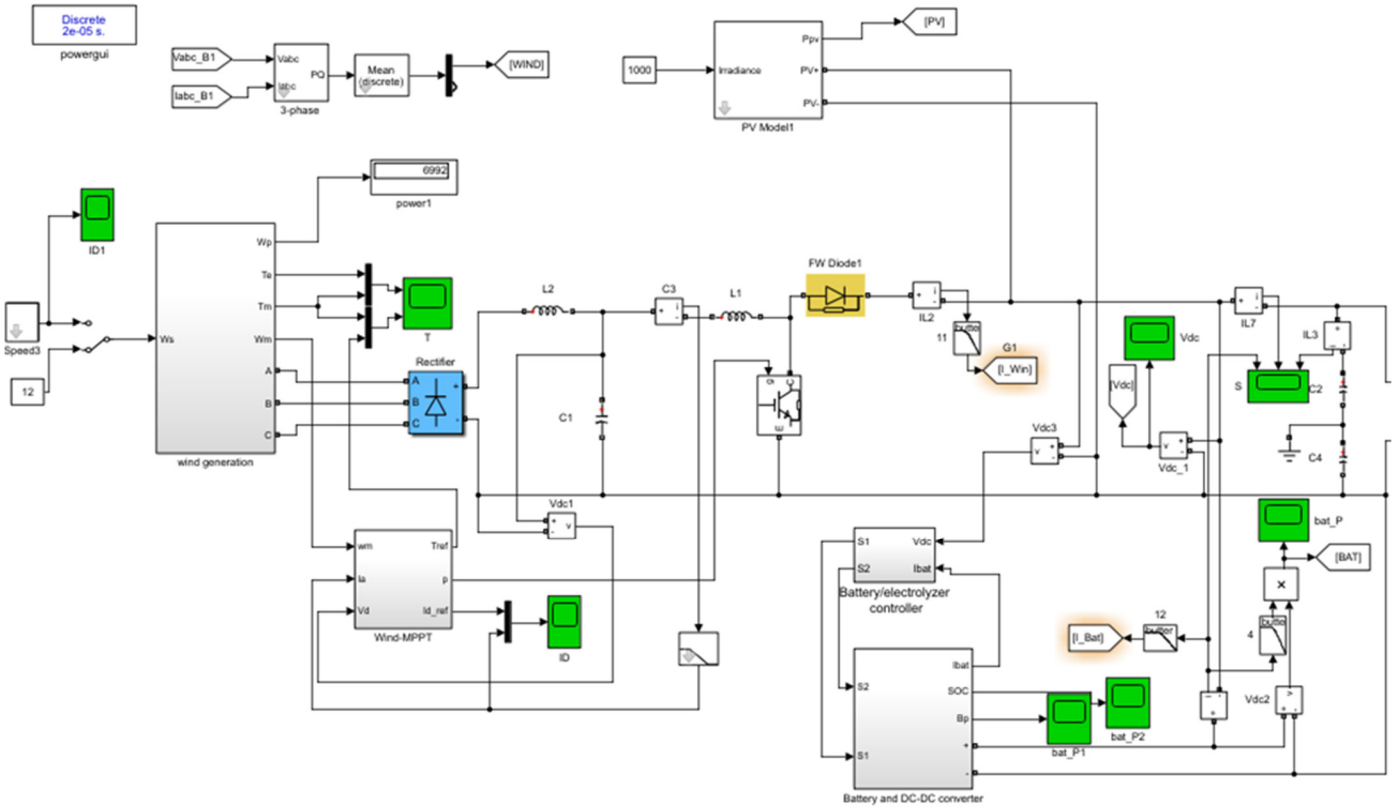


Figure 12. PV-wind hybrid microgrid system input DC side in MATLAB/Simulink.

5.1. System Parameters

The main block parameters for the PV model are shown in Figure 13. The maximum voltage of 666.6 V is obtained by connecting 22 modules in series at a maximum voltage of 30.3 V. The block parameters display the open-circuit, short-circuit, and current at Pmax values. The current in the short circuit is 8.01 A. The DC microgrid is mostly supplied by the PV system. Using a solar panel, solar energy is converted into electrical power. To replicate DC sources in the system design, PV arrays are coupled via a boost converter. Because it depends on temperature, irradiance, and load characteristics, a PV system's output voltage is not optimal.

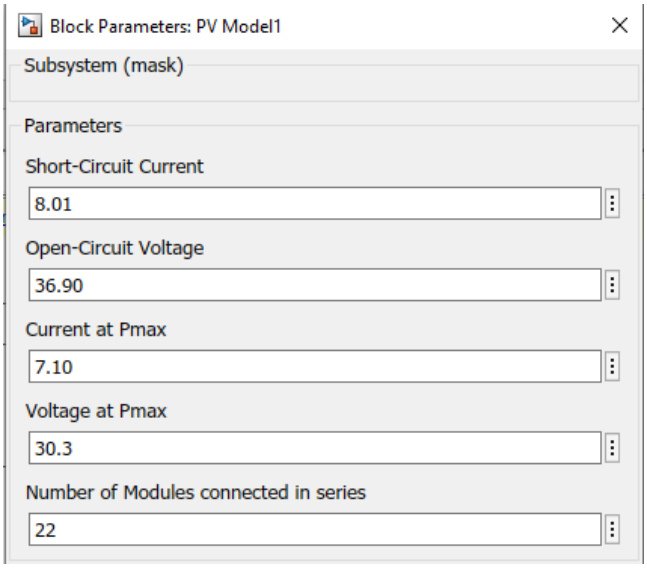


Figure 13. PV model main block parameters.

All of the values for the nominal mechanical output power (W) at 0.8 Pu, the base power of the electrical generators (VA), and the base wind speed (m/s) of a wind turbine at 12 m/s are shown in Figure 14, which displays the wind turbine model block parameters. The DC microgrid is also powered by wind energy. The goal of this study is to generate DC output as wind generation (alternating current) is transformed into direct current using a rectifier. There is a clear correlation between wind speed and electricity generation; as wind speed increases, so does power generation. Wind-generated power is always changing. Non-fluctuating power must first be stored in a battery before being applied to the load. The simulation results of wind turbines utilizing PMSG are represented by the Tm and Te which are shown in the simulations.

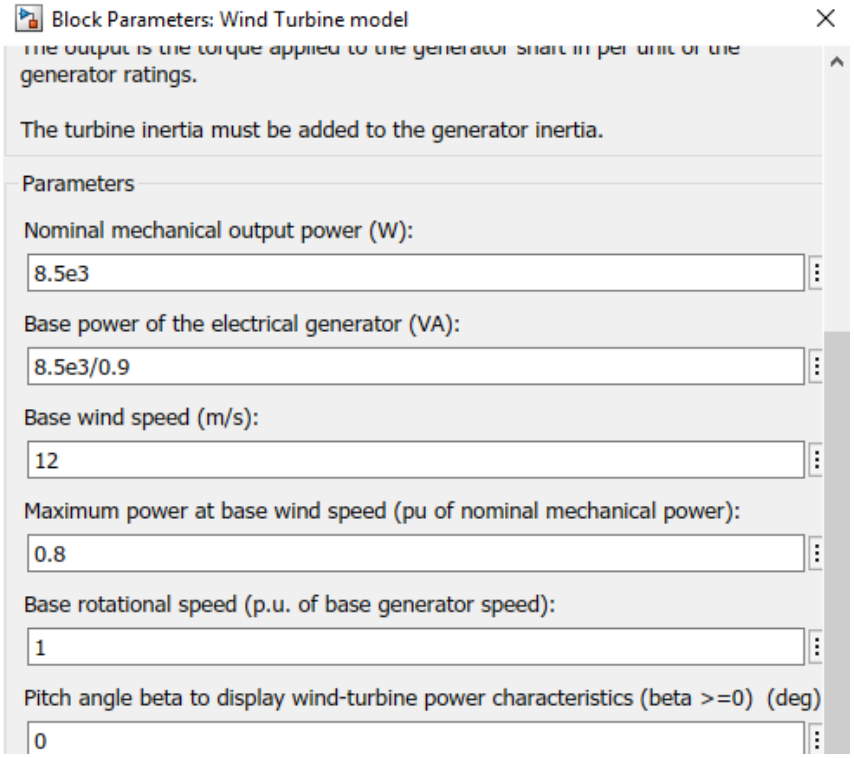


Figure 14. Wind turbine model main block parameters.

The battery storage main block parameters are shown in Figure 15 below. A nickel-metal-hydride with a rated capacity of 6.5 Ah and a nominal voltage of 300 V is presented. The battery storage is coupled to an average-model DC/DC converter. An essential component of energy storage in a DC microgrid is battery storage. For energy storage, a battery is connected to DC via a bi-directional DC/DC converter. In order to increase efficiency and preserve voltage stability, a microgrid that relies on distributed energy resources must have an energy storage system.

The parameters of the rectifier block are shown in Figure 16. In order to convert alternating current to direct current, the rectifier is essential. To get the most power out of the wind resource, the blades revolve at different speeds; as a result, the electricity is converted from AC to DC at a particular frequency. The DC voltage that fluctuates at the same frequency as the AC input is the rectifier's output. Since rectifier parameters are a gauge of the effectiveness of the rectification process, they are extremely important. The rectifier main employs capacitance and diode snubber resistance as shown, and its forward voltage is 0.8 V. A rectifier display's block main parameter at snubber resistance is set to 100 ohms. Additionally, the initial value of the snubber capacitance is shown.

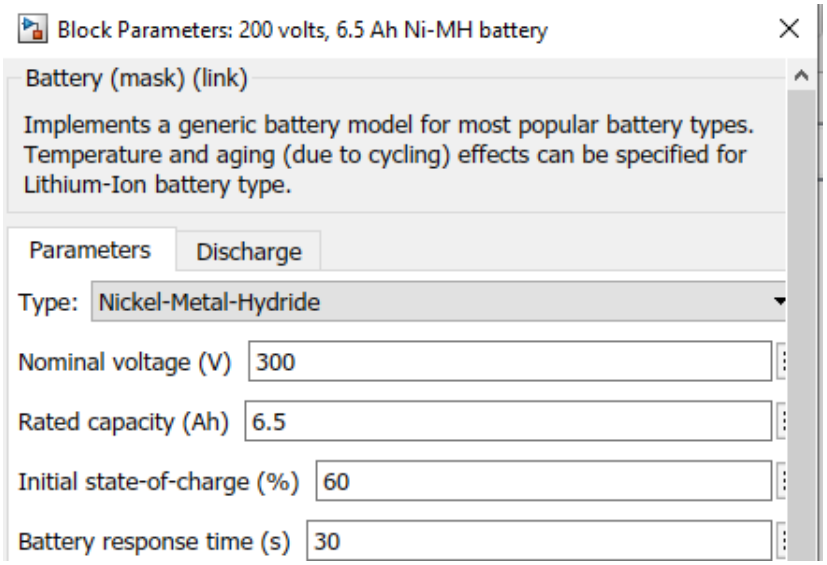


Figure 15. Battery storage main block parameters.

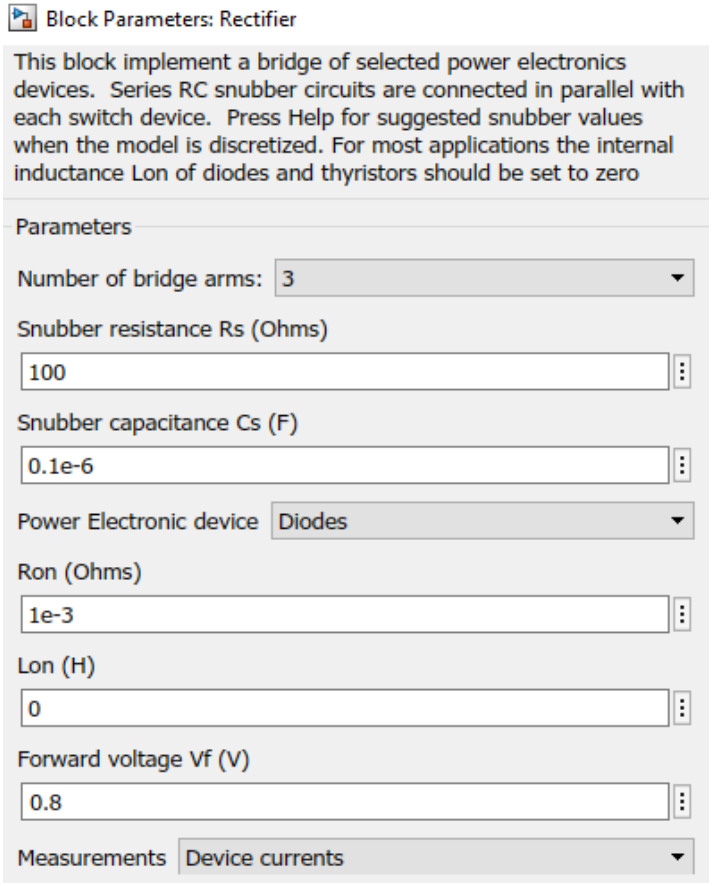


Figure 16. Rectifier block parameters.

5.2. Case 1: Wind Turbine Internal Analysis

Turbines use wind energy to convert AC into DC output. The first simulation shows the RMS line current under typical conditions. Since the electricity generated by wind turbines is proportional to the cube of the wind speed, they should be positioned in areas with high mean annual wind speeds. Figure 17 shows the RMS line current (ILine_RMS), AC power, and line current (ILine). From t = 0.0623 s to t = 0.24 s, there are anomalous current occurrences. During this time, the current spikes upward and surpasses 22 A. As

the system continues to function, the current stabilizes at t = 0.25 s at roughly 12 A. The second simulation shows the power (Pac) in normal conditions. Generator-generated AC is transformed into DC by rectifiers and then sent to a DC bus. The system begins steadily between 0.01 and 0.125 s, then it climbs until it reaches 20,000 kW. At t = 0.25 s, the power drops below 10,000 kW and then reaches 20,000 kW, returning to normal and maintaining a consistent power level throughout. The current in line a (ILine) is shown in the third simulation. The current between 0 s to 0.25 s is not stable, reaching 50 A; in the next phase, 0.5 to 1 s, the current is stable at 25 A. During the last phase, 1 to 1.5 s, the current is stable and the system is performing very well.

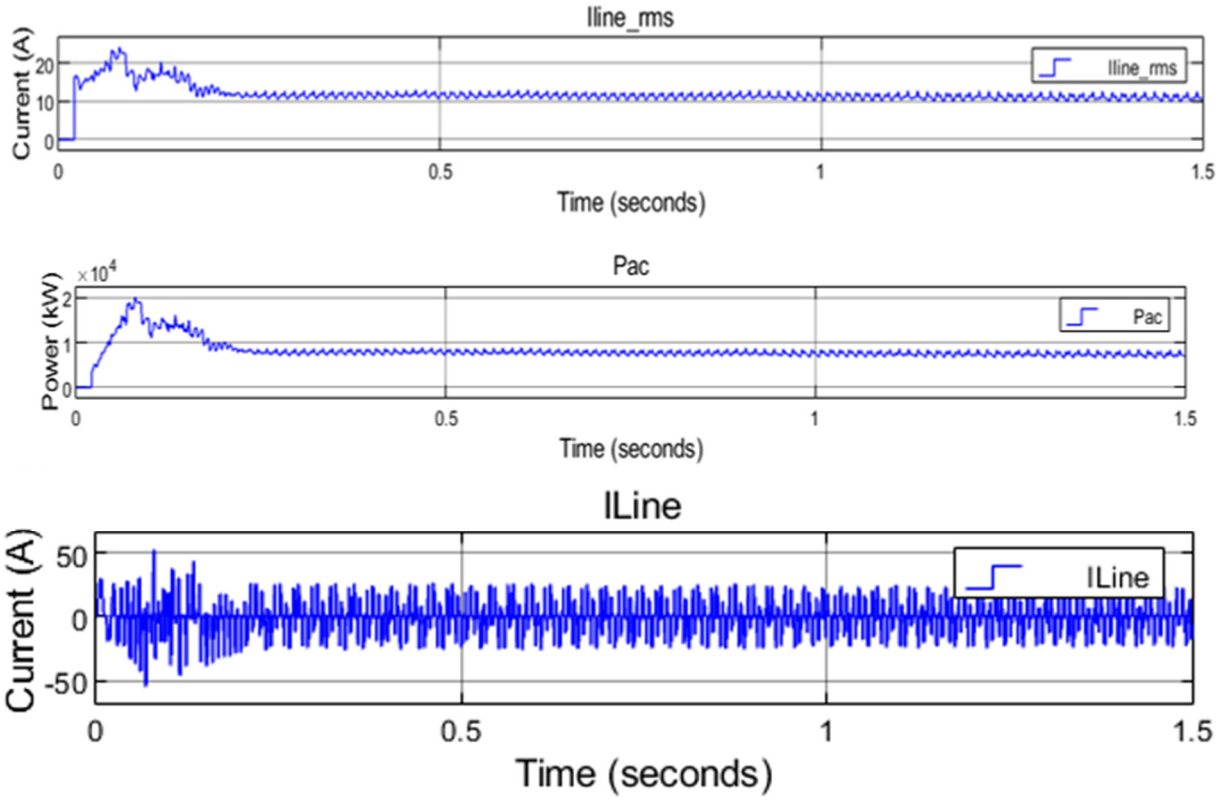


Figure 17. RMS line current (ILine_RMS), AC power, and line current (ILine).

The wind generation/Te with wind generation/Tm output and wind generation/Te with wind generation/Tm output under normal conditions are shown in Figure 18. According to these models, wind generation lacks power stability before t = 0.2 s, when it rises to 120 V, and exhibits power stability at t = 0.25 s, when it falls to 40 V. Te remains at 70 V. To attain high efficiency in a wind power conversion system, the Maximum Power Pointer Tracker (MPPT) independently regulates each boost in a variable speed operation system. The range in which rotor angular velocity control is required, which varies depending on the turbine, determines the employment of controllers.

Figure 19 displays the wind-MPPT/1 output and wind-generation/Tm under normal conditions at equilibrium. When wind-MPPT/1 is coupled, simulations show that, before reaching equilibrium at t = 0.25 s, wind-MPPT/1 rises from 0 V and surpasses 50 V, while wind generation/Tm falls from 120 V until both reach 40 V. Within the functioning range of the wind turbine, the speed control rotor is used for MPPT. To attain high efficiency in a wind power conversion system, each boost is managed by a separate MPPT in a variable speed operation system.

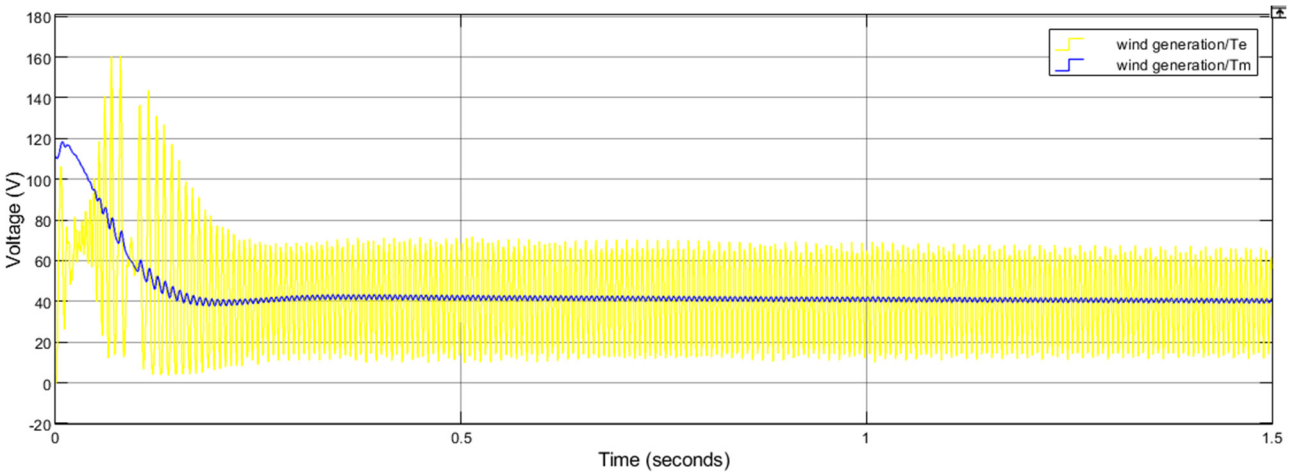


Figure 18. Wind generation/Te with wind generation/Tm.

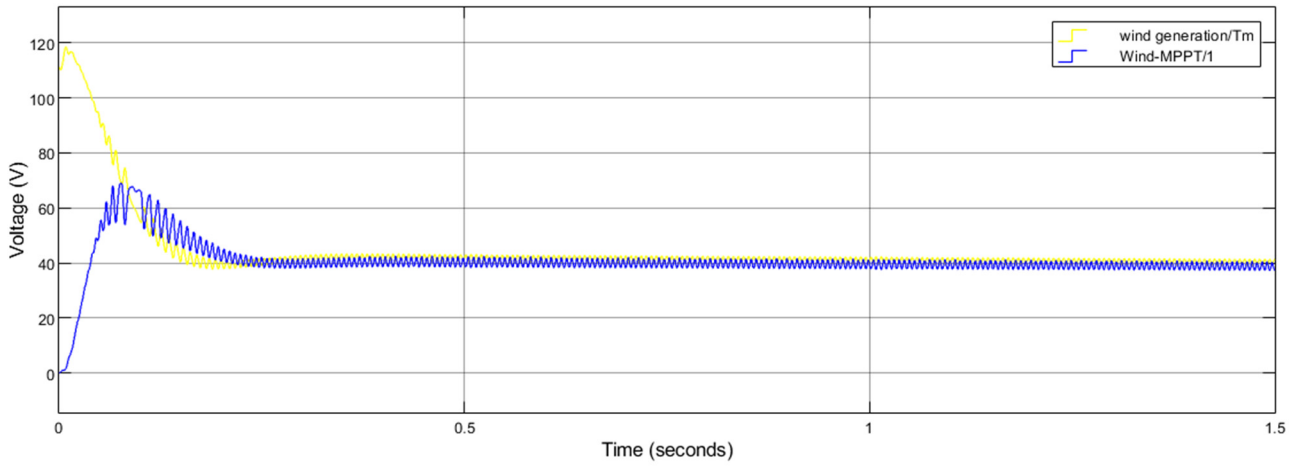


Figure 19. Wind-MPPT/1 output and wind-generation/Tm.

5.3. Case 2: No Phase Condition

Figure 20 illustrates a total harmonic distortion 3 (THD3). Each unit has a variable and blown voltage as a result of the large waves caused by faults on the consumer and voltage sides. The fault initially achieves the maximum output voltage of 1.1 pu; however, over the 0–0.5 s interval, the voltage fluctuates between 0.18 pu and 0.5 pu. The rated value of this condition is delayed in returning to stability due to the defect. At t = 0.501 s, the output remains steady at 0.1 pu until t = 1 s, at which point a slight impact is observed, but the system finally recovers to normal.

The summary of a hybrid DC microgrid under power flow for wind generation is presented in Table 2.

Figure 21 shows V and I pu from inverter and LC measurement. The three measurements are at equilibrium all at 0.25 pu. The development of inverter-based micro-grids is necessary because of the anticipated expansion of small-scale non-50/60 Hz power sources and the desire to be able to support loads independently of the main electrical grid. Different operation, control, and protection strategies are needed for power electronic interfaces because they have characteristics that are considerably different from those of normal electrical devices.

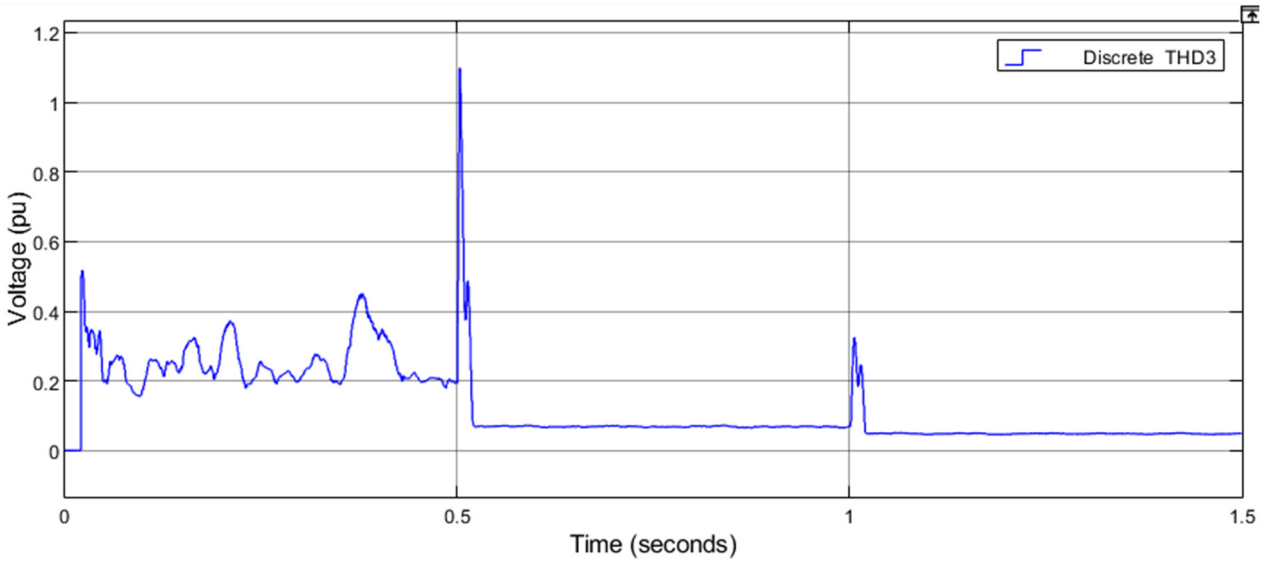


Figure 20. Total harmonic distortion 3 (THD3).

Table 2. Power flow results for wind generation.

Wind Generation	
Conditions	**Outputs**
RMS Line current (ILine_RMS),	22 A
AC Power	20,000 kW
Line current (ILine)	25 A
Wind generation/Te with wind generation/Tm	Te = 70 V Tm = 40 V
Wind generation/Tm and wind MPPT/1 output during normal condition	Tm = 120 V MPPT/1 = 70 V Equilibrium = 40 V
Total Harmonic distortion 3 (THD3)	THD = 0.1 pu

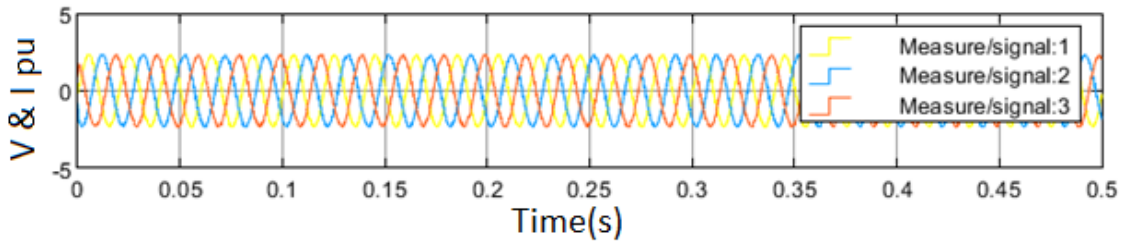


Figure 21. V and I pu. from inverter and LC measurement.

The measure of LC filter and control of inverter simulated at Vabc and Iabc through V and I pu is shown in Figure 22. The first port is connected to IL1, where the output is parallel to RMS discrete and THD discrete. The current and voltage is shown in (x; y) value format. The results revealed constant growth with no variations: (0.0395; −1.51082), (0.2098; −2.07678), (0.3184; 2.30139), and (0.4035; 0.219526). The system output voltage and current signals of the microgrid are not significantly distorted and the output currents are appropriately limited. Although the feedforward term is not necessary, it does improve transient voltage performance, demonstrating that difficulties with noise and accuracy are resolved. In some networks, single-phase harmonically distorting loads predominate, so it

is important to pay attention to these networks' control strategies for preserving voltage quality. Examined and contrasted with both conventional power systems and control of DC/DC power converters is a control strategy that takes advantage of the controllability of inverters to operate a micro-grid and deliver good power quality.

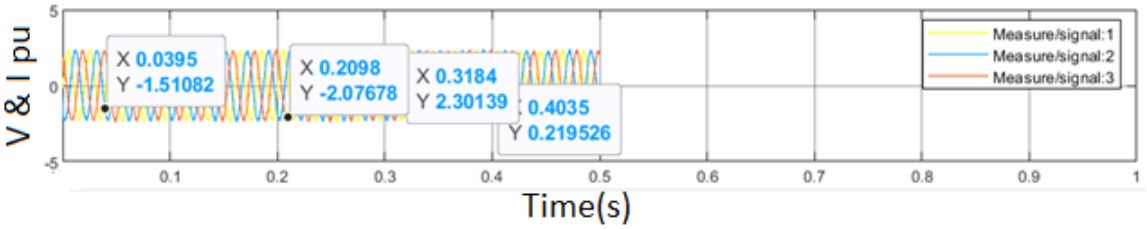


Figure 22. V and I pu. from inverter and LC Filter.

Figure 23 shows the Vph_max simulation during inverter simulation. In this case, the three presented responses are within 5% of the zone, and at t = 0.05 s and t = 0.22 s, one demux is extremely low below 0.98 pu. Initially, it hits the max 1.02 pu, and decreases until t = 0.025 s. The out shift displays the same sequence but with a regular spike in between. To verify the thorough model utilized in the simulation, the corresponding dynamic responses in active power, voltage, current, and frequency are displayed. The method utilized in the simulations can be used for interface control of massive grid-connected battery energy storage systems as well as low voltage ride-through of solar PV-wind based grid-connected microgrids.

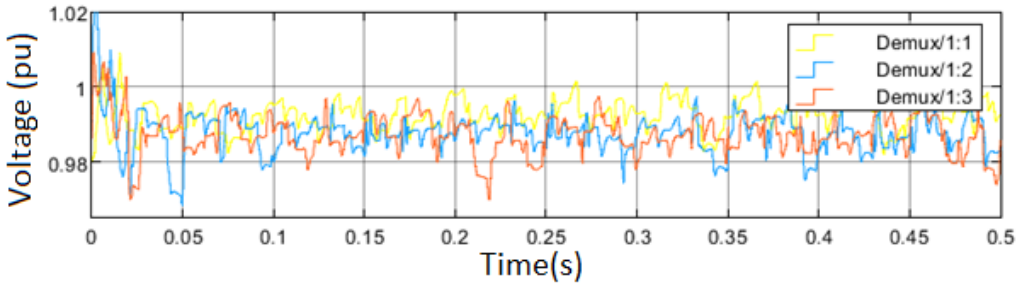


Figure 23. Vph_max during inverter simulation.

In Figure 24 the microgrid output changes according to the load demand increase as a result of the response from the inverter-controlled simulation under VL-L. The three demux/2 are at equilibrium throughout the response. The output is distributed evenly after the inverter control. A maximum of 500 V delivered constantly. These pulses correctly alter the operating mode of the switching control system and initiate the switching function of the IGBT-based switch. In order to evaluate the suggested technique for balanced voltage sag, the main grid fault, triple-phase to the ground, is employed to create a 50% voltage sag.

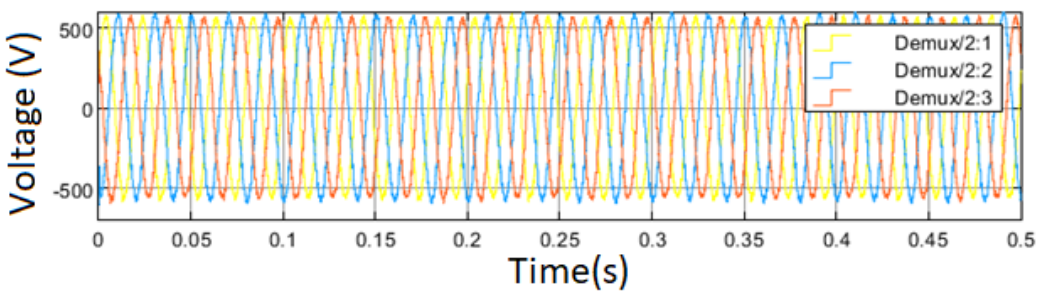


Figure 24. VL-L inverter simulation.

The instant power mismatch and droop control properties, however, change in the island mode. Figure 25 shows Vph_rms, the inverter output controller's optimization process. The voltage and current controllers for the system are identical PI controllers. The phase voltages shift sharply up before t = 0.05, 230 V is exceeded above the standard, and after that, the system is stabilized constantly at 230 V. At t = 0.23 s, there is a spike of demux/3:3, but the system retains a composed state and remains within the appropriate scale. Figure 16 shows the magnitude of the voltage sag on the main grid, which results in a commensurate increase in the current amplitude. The secondary power reference is integrated into the secondary control system.

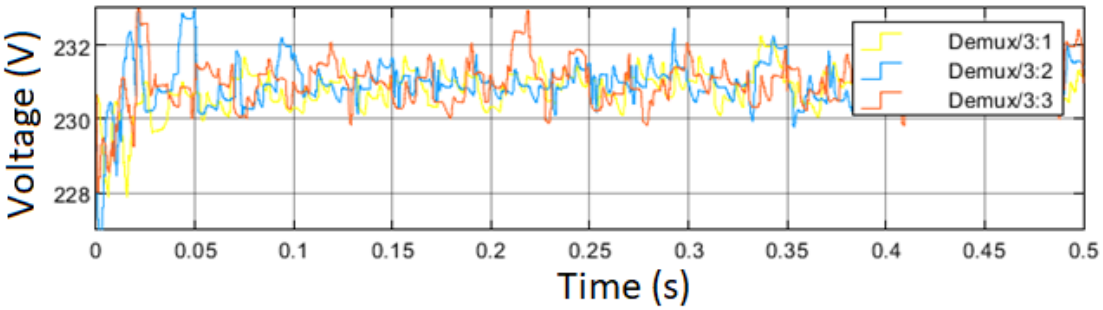


Figure 25. Vph_rms inverter.

The system frequency and bus RMS voltage variations during the simulation can be seen in Figure 26, which shows the Vlin for the LC filter, Subsystem 1/2. Under this, the bus us voltage and frequency of a system frequency is kept well within the nominal range. In off-grid connected mode, at t = 0.05 s, it hits the maximum of 600 V. As a result, the IGBT-diode switched reactor is simultaneously switched in series with all phases for balanced transient conditions and in series with the affected phase for unbalanced conditions, activating the strategy scheme mode operation.

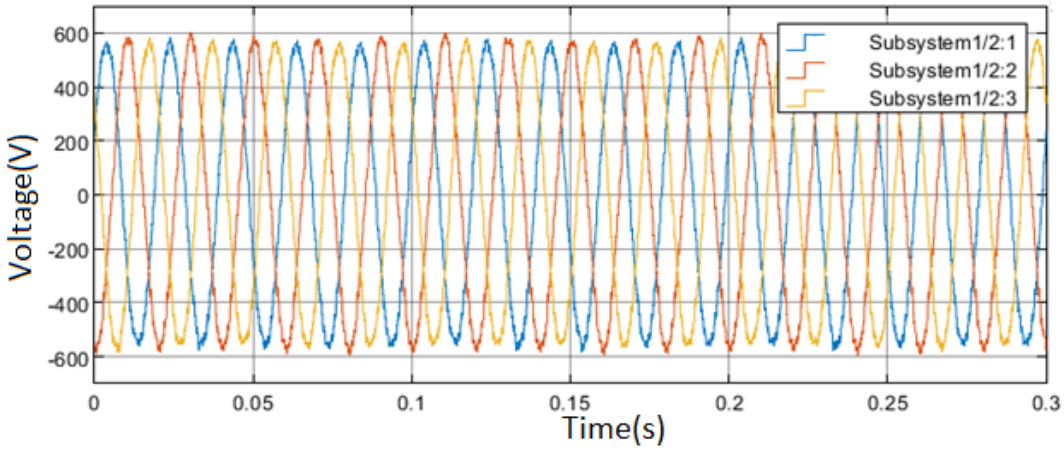


Figure 26. Vlin LC filter for subsystem 1.

The control of the inverter plays a dynamic part in coordinating m,V results. The pulses from the control circuit send the signal back to PMW IGBT inverter1. Figure 27 shows a V pu during inverter simulation. The Vabc and Vabc_inv are important components when combined with all other parameters taken into consideration in this study. RMS discrete is an important tool to control the circuit. The initial phase voltages after the start is 1.02 pu for demux/1:2 which is the highest, whereas others are below 1.01 pu. At t = 0.025 s, the voltage is below 1 pu and remains constant until it spikes above 1 pu at t = 0.325. The results depict that at t = 0.375 s, it returns to normal and is below 1 pu.

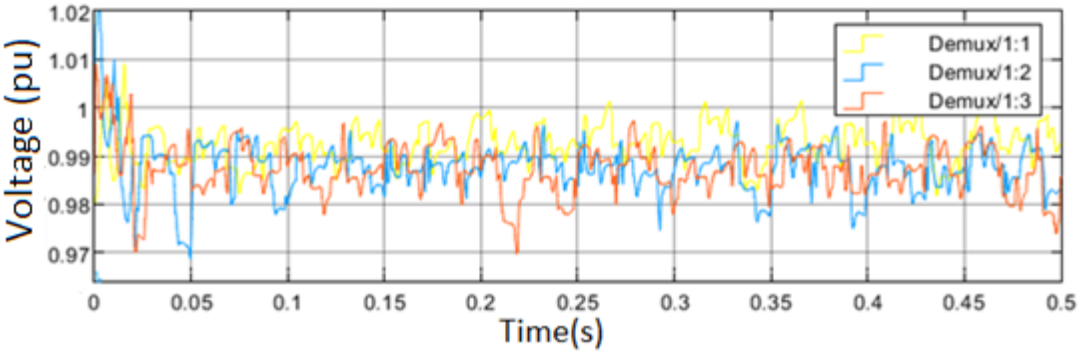


Figure 27. V pu during inverter simulation.

The system displays the unstable condition of the voltage Vph_rms from the inverter control filter circuit. The RMS discrete vab1, 2, and 5 plays an important part in smothering and boosting the output voltage. Figure 28 shows a Vph_rms inverter from the control circuit. The Vph_rms inverter spikes and hits 233 V at t = 0.025 s for all the parameters, and at t = 0.05 s for only demux/3:2. At t = 0.225 s, only demux/3:3 is at peak and reaches 233 V. The results show no consistency throughout the entire stage. Despite main grid transient conditions, the microgrid voltage is corrected for the efficient operation of the microgrid through the deployment of the proposed strategy schemes for hybrid microgrids. The microgrid's voltage has increased. As a result, Figure 26 shows a seamless change from a system and disorder situation. Consequently, as illustrated, the output current of the LC filter for DERs is appropriately limited.

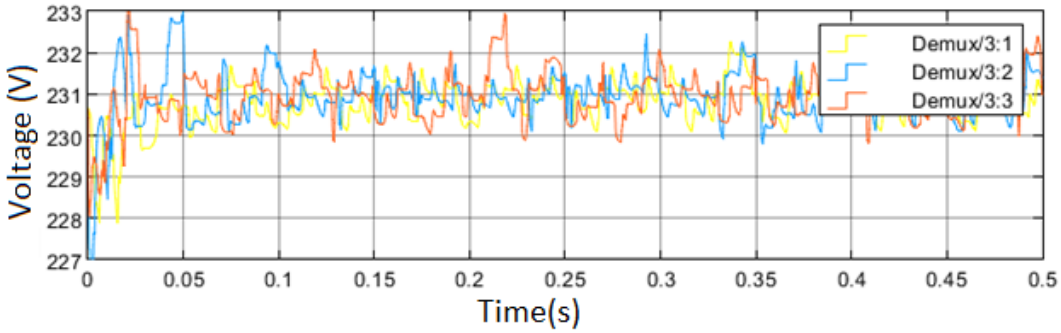


Figure 28. Battery performance Voltage Simulation.

5.4. Case 3: Data Inspector Power Quality Analysis

This section provides data inspection for power quality analysis battery performance summary in all the figures below. Figure 29 shows battery performance. Figure 30 shows battery and wind system performance. Figure 31 shows output power. Figure 32 shows backup power and generator terminals. Figure 33 shows system stability. Figure 34 shows Vph_rms, m, and Vlin performance. Figure 35 shows Vph_rms inverter performance. Figure 36 shows overall performance in terms of m. The inverter output performance is shown in Figure 37. Figure 38 depicts V and I per-unit performance summary. Figure 39 shows ITHD performance. Figure 40 depicts the VL-L performance summary.



Figure 29. Battery performance.

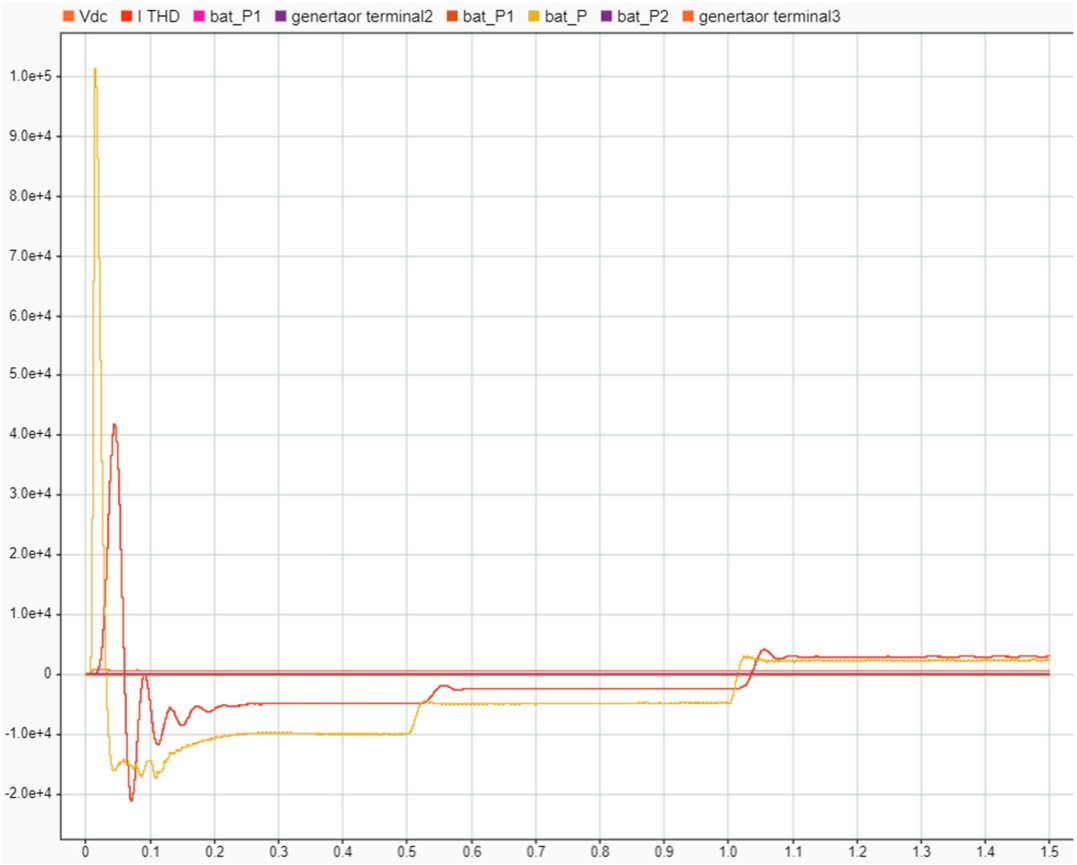


Figure 30. Battery and wind system performance.

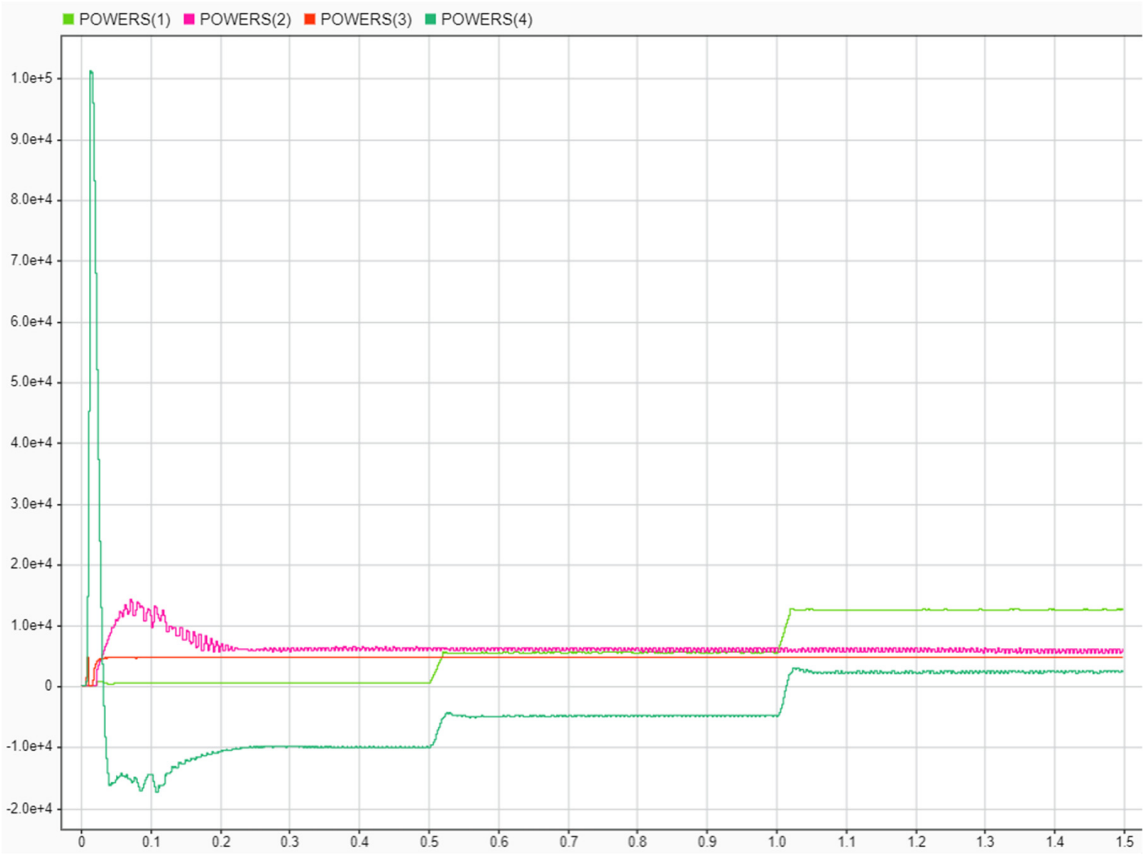


Figure 31. Output power.

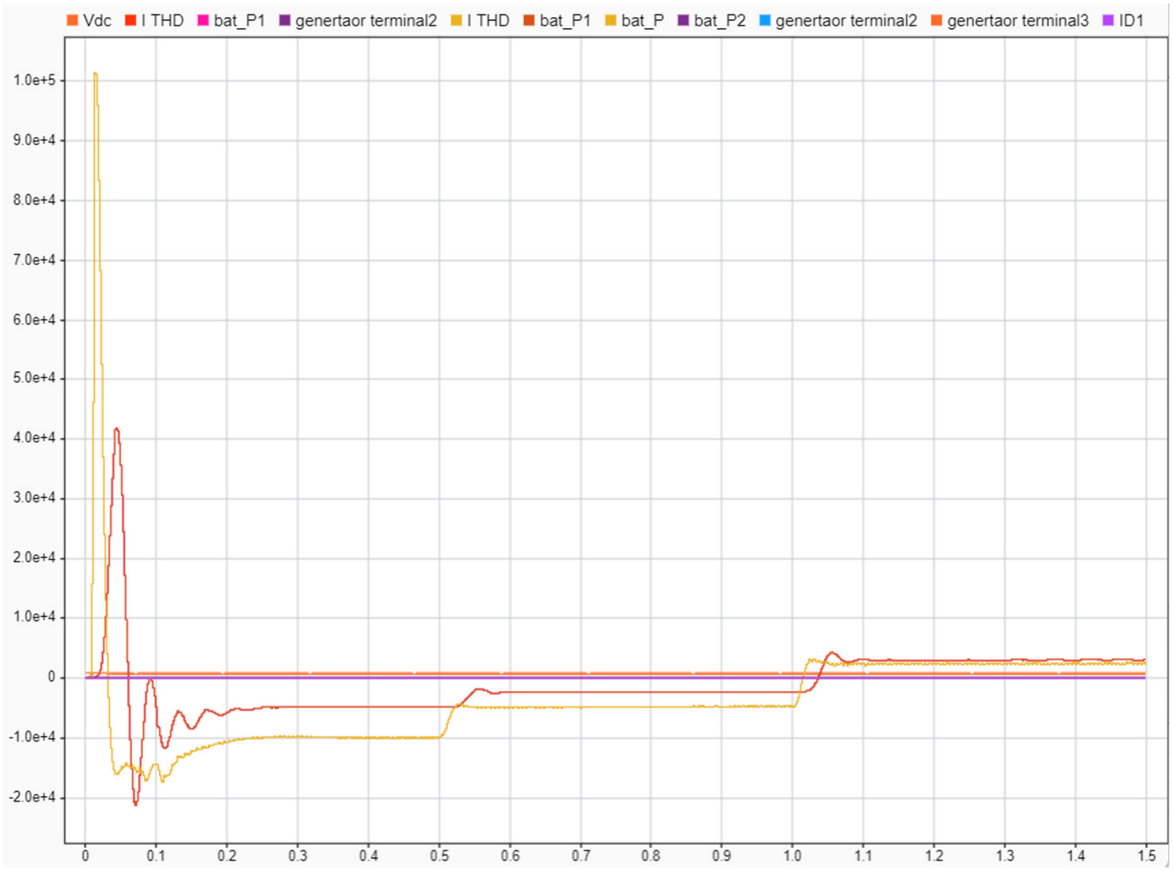


Figure 32. Backup power and generator terminals.

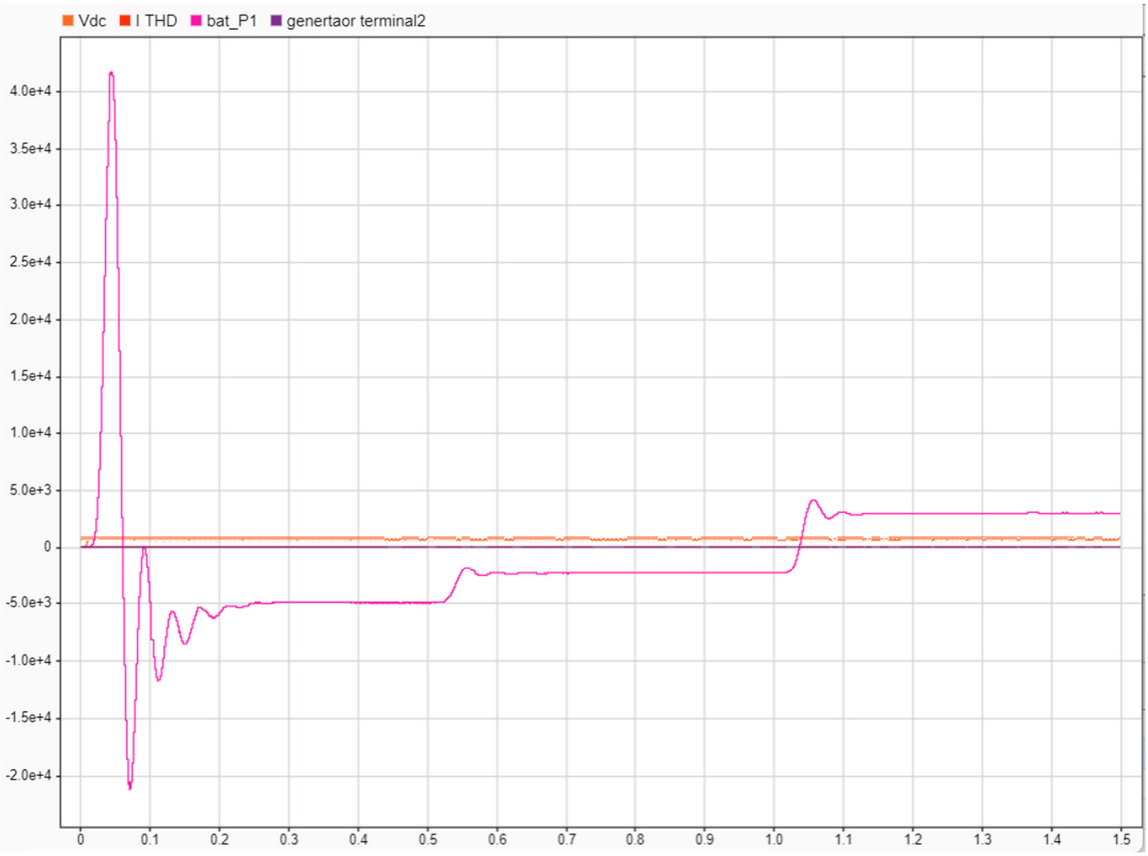


Figure 33. System stability.

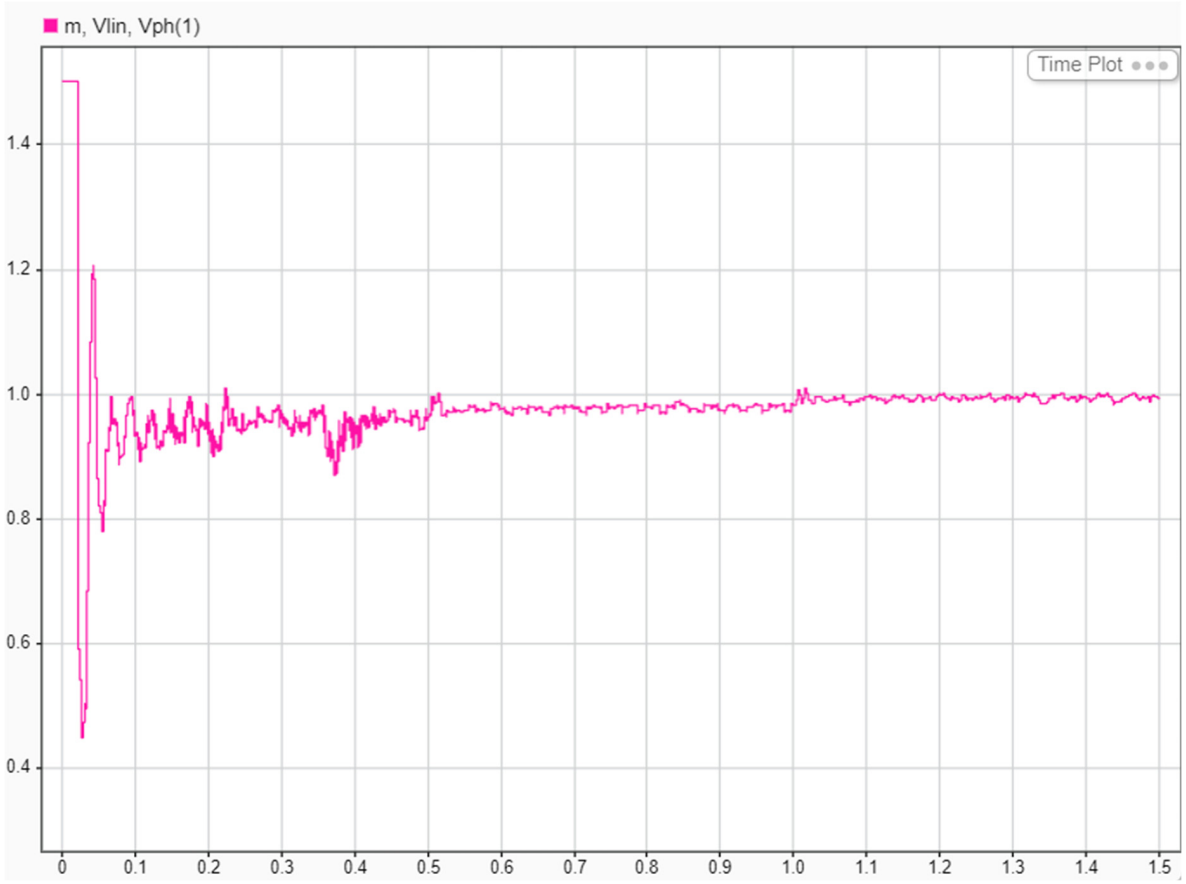


Figure 34. Vph_rms, m, and Vlin performance.

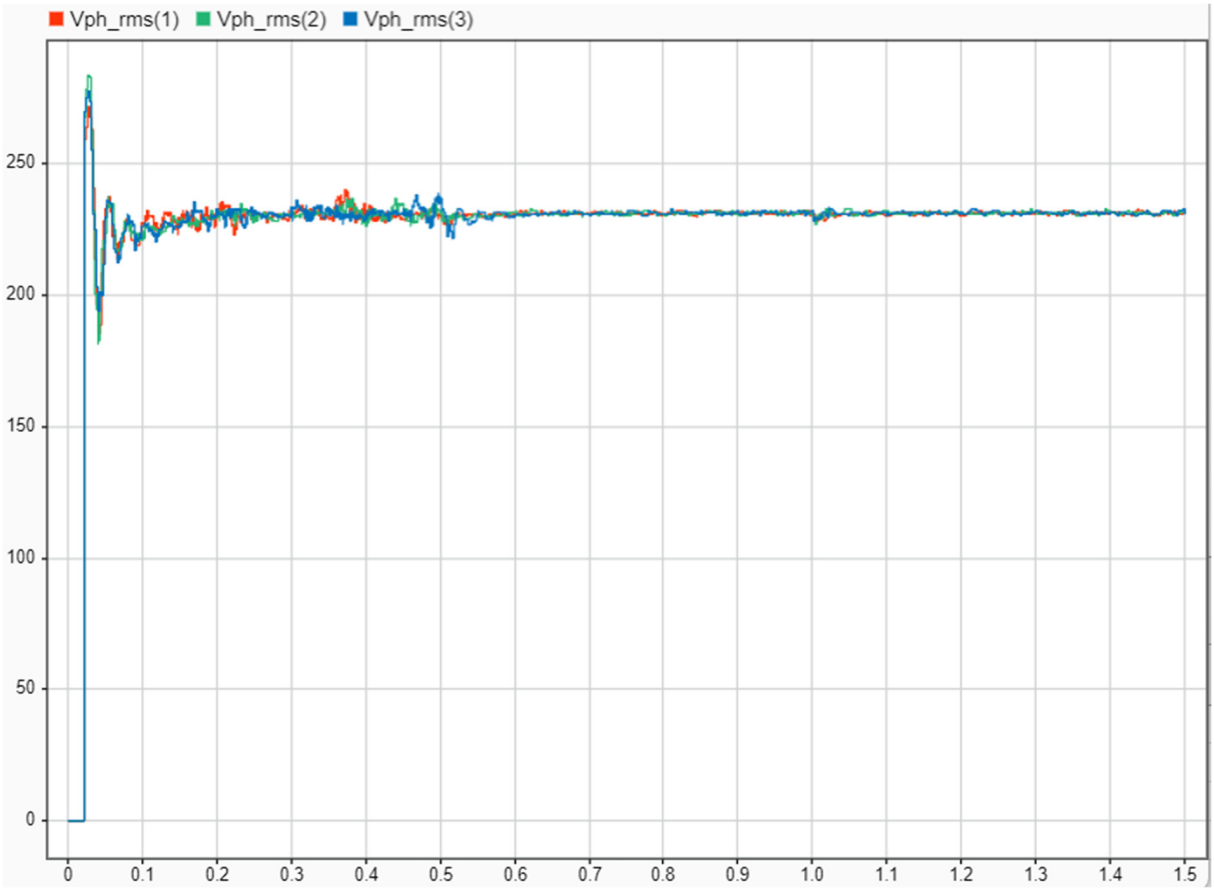


Figure 35. Vph_rms inverter performance.

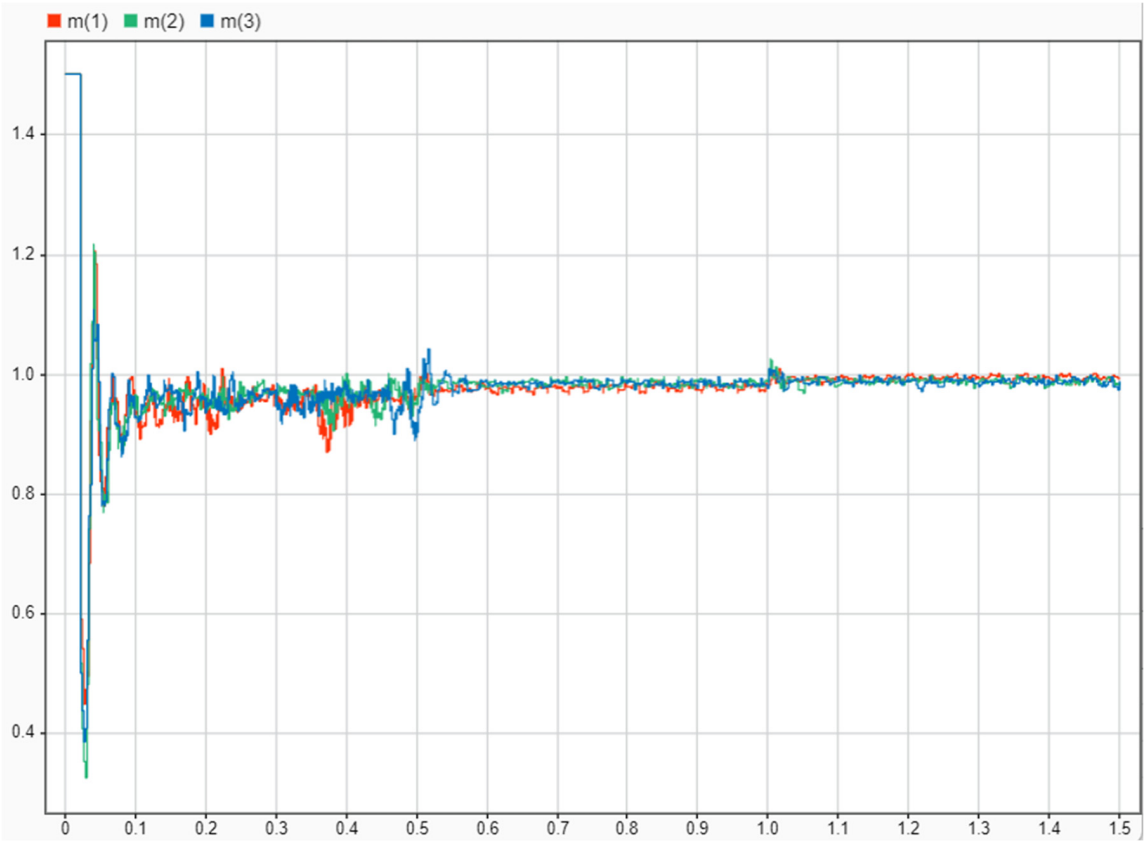


Figure 36. m overall performance.

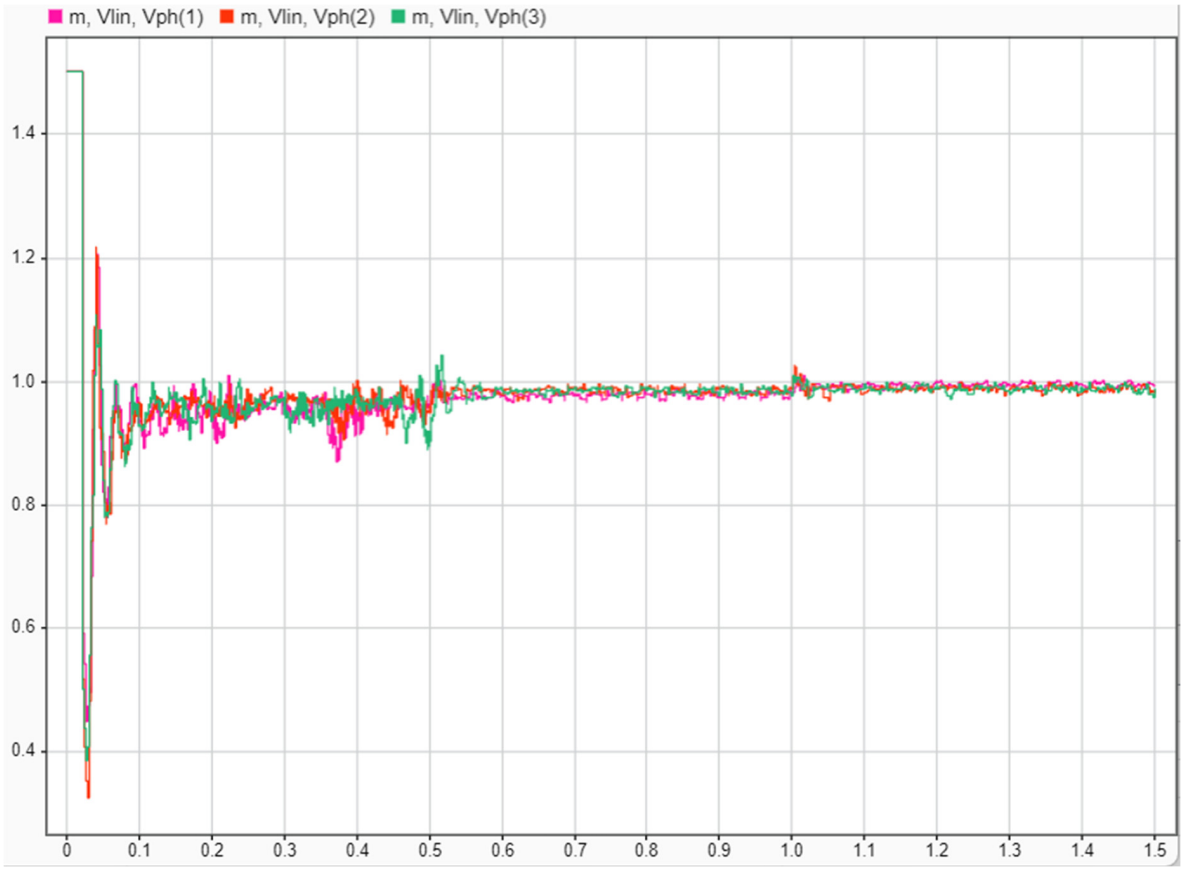


Figure 37. Inverter output performance.

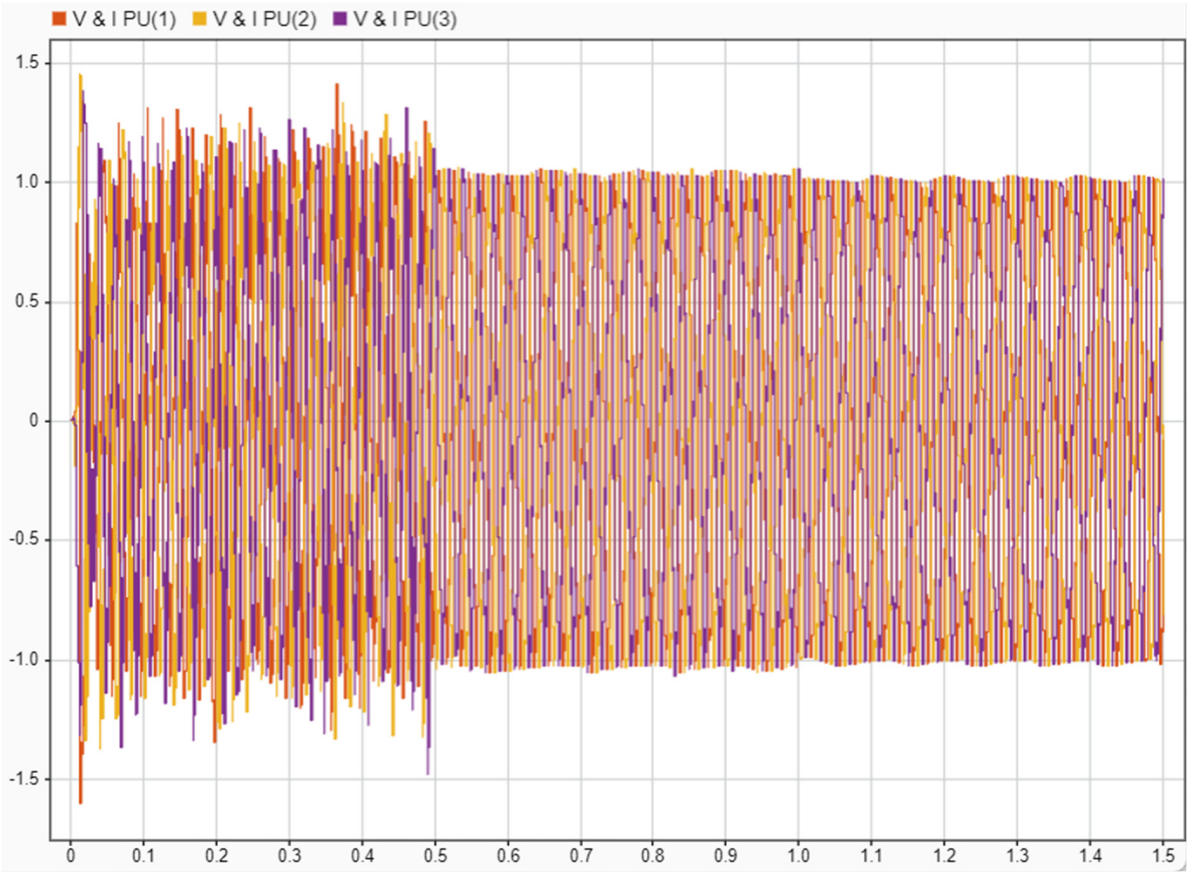


Figure 38. V and I per-unit performance summary.

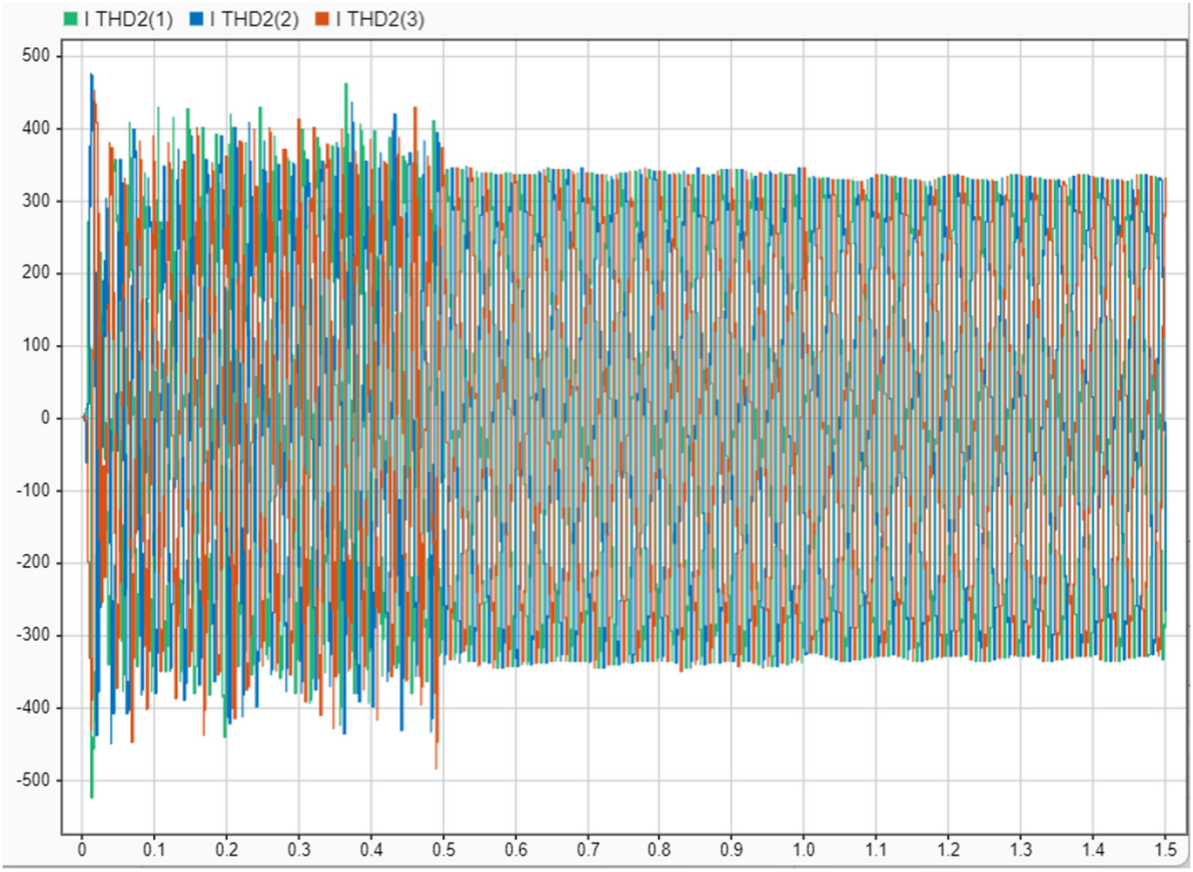


Figure 39. I THD performance.

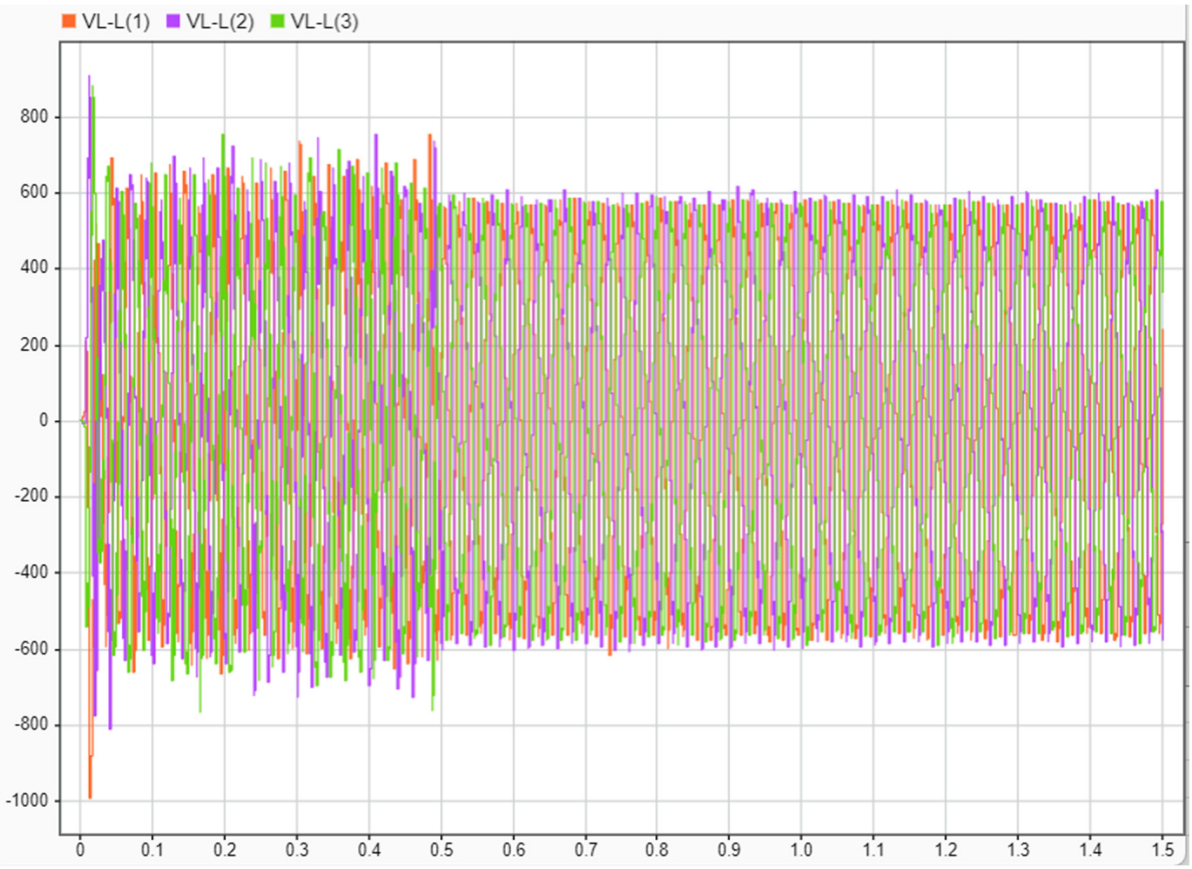


Figure 40. VL-L performance summary.

6. Conclusions and Future Outlook

This study focuses on developments in the use of microgrid systems with PV-wind-generating units, with a particular focus on the relevant microgrid control systems, methods, and concepts. To address the control issues of PV-wind hybrid generation microgrid systems, ICANN in microgrid has been proposed as a workable solution by integrating appropriate artificial intelligence algorithms. Research in this area has taken several paths, such as optimizing the performance of a hybrid microgrid system through the use of artificial intelligence and other algorithms inspired by nature. This paper presents the design and optimization of microgrid DG controllers. These controllers can automatically determine how much electricity to share, allowing the microgrid to settle rapidly. This paper also focuses on migration, and the increase in renewable energy investment illustrated in this report makes it abundantly clear that renewable energy is the way of the future. Of the United Nations' Sustainable Development Goals, SDG 7 has the potential to be considerably aided by artificial intelligence-based systems. The standalone functioning of a microgrid is rather difficult, given that the interface inverters are supposed to manage the voltage and frequency of the islanded system. Hybrid voltage source control is created by combining droop control and virtual impedance with the interface power electronic inverters' normal grid forming control. The results show that this control improves power regulation even when the load changes. Because of the vigorous nature of normal electrical loads, dynamic adjustments of control parameters are required to keep up with the changing microgrid load status. The inverter and LC filters play a vital role. The results demonstrate that even when the load varies, this control enhances power regulation, making the use of AI solutions for improvement necessary. The results of the smart grid simulation are excellent, and applying AI will improve performance. Inverter control can be used to achieve coordination across numerous DGs in a microgrid system combined with AI strategies. The ICANN technique is applicable and can improve the performance of the system. It has been demonstrated that heuristic approaches have consistently outperformed classical approaches. The effective use of AI technology makes it feasible to create systems with high AI performance or other characteristics that might not be compatible with traditional methods. Coordination between many DGs in a smart grid system can be achieved using inverter control.

The future outlook is based on the Sustainable Development Agenda for 2030, which was endorsed by all UN members, and offers a strategic roadmap for global peace and prosperity. Regardless of their economic situation, all countries are urged to act by implementing these 17 Sustainable Development Goals (SDGs). This paper's main topic is SDG7, which asks for universal access to cheap, clean energy. This makes the development of an assessment tool to gauge nations' progress toward SDG7 necessary. Cutting-edge technological advances are being made in artificial intelligence (AI). Due to their extensive acceptance across several industrial sectors and verticals, concerns related to sustainability, fairness, inclusivity, efficiency, and usability in relation to these technologies are now a top concern for international consumers and producers. Particle swarm optimization (PSO), fuzzy logic (FL), artificial neural networks (ANNs), and ant bee colony (ABC) are a few AI techniques that have revolutionized the field of power electronics and power engineering. These techniques provide powerful tools for design, simulation, control, estimate, fault diagnostics, and fault-tolerant control in today's smart grid (SG) and renewable energy systems (RES). It is crucial to have access to clean energy. Despite this, many developing countries lack clean energy for their regular domestic duties, especially those in the sub-Saharan Africa region. In order to improve the performance of smart grids, the study of reviews and applications of AI is very crucial.

Author Contributions: This article is part of the Ph.D. work of M.L.T.Z., which is supervised by R.S. and co-supervised by R.T.; both supervisors R.S. and R.T. contributed substantially to the manuscript and the research that forms part of the study and writings. Conceptualization, M.L.T.Z., R.S. and R.T.; methodology, M.L.T.Z.; software, M.L.T.Z.; validation, R.S. and R.T.; formal analysis, R.S. and R.T.; investigations, M.L.T.Z.; resources, M.L.T.Z.; data curation, M.L.T.Z.; writing—original draft preparation, M.L.T.Z.; writing—review and editing, M.L.T.Z.; visualization, R.S. and R.T.; supervision, R.S. and R.T. All authors have read and agreed to the published version of the manuscript.

Funding: This research received no external funding.

Data Availability Statement: The authors have published research data available on Google scholar.

Acknowledgments: The authors are truly indebted to all the cited and not cited researchers around the world who have made contributions to the field of applications of artificial neural network techniques in microgrid for power quality improvement.

Conflicts of Interest: The authors declare no conflicts of interest.

References

1. Salim, H.K.; Padfield, R.; Hansen, S.B.; Mohamad, S.E.; Yuzir, A.; Syayuti, K.; Tham, M.H.; Papargyropoulou, E. Global trends in environmental management system and ISO14001 research. *J. Clean. Prod.* **2018**, *170*, 645–653. [CrossRef]
2. Simon, C.A. *Alternative Energy: Political, Economic, and Social Feasibility*; Rowman & Littlefield Publishers: Lanham, MD, USA, 2020.
3. Ediger, V.Ş. An integrated review and analysis of multi-energy transition from fossil fuels to renewables. *Energy Procedia* **2019**, *156*, 2–6. [CrossRef]
4. Zulu, M.; Ojo, E. Power Flow and Fault Analysis Simulation For A PV/Wind Hybrid DC Microgrid. In Proceedings of the 2022 30th Southern African Universities Power Engineering Conference (SAUPEC), Durban, South Africa, 25–27 January 2022; IEEE: Washington, DC, USA, 2022; pp. 1–6.
5. Kumar, M. Social, economic, and environmental impacts of renewable energy resources. In *Wind Solar Hybrid Renewable Energy System*; IntechOpen: Rijeka, Croatia, 2020; Volume 1.
6. Murdock, H.E.; Gibb, D.; André, T.; Sawin, J.L.; Brown, A.; Ranalder, L.; Collier, U.; Dent, C.; Epp, B.; Hareesh Kumar, C. Renewables 2021-Global Status Report. 2021. Available online: https://www.ren21.net/wp-content/uploads/2019/05/GSR2021_Full_Report.pdf (accessed on 26 May 2025).
7. Vinuesa, R.; Azizpour, H.; Leite, I.; Balaam, M.; Dignum, V.; Domisch, S.; Felländer, A.; Langhans, S.D.; Tegmark, M.; Fuso Nerini, F. The role of artificial intelligence in achieving the Sustainable Development Goals. *Nat. Commun.* **2020**, *11*, 233. [CrossRef] [PubMed]
8. Alipour, R.; Alipour, R.; Fardian, F.; Koloor, S.S.R.; Petrů, M. Performance improvement of a new proposed Savonius hydrokinetic turbine: A numerical investigation. *Energy Rep.* **2020**, *6*, 3051–3066. [CrossRef]
9. Buonocore, J.J.; Choma, E.; Villavicencio, A.H.; Spengler, J.D.; Koehler, D.A.; Evans, J.S.; Lelieveld, J.; Klop, P.; Sanchez-Pina, R. Metrics for the sustainable development goals: Renewable energy and transportation. *Palgrave Commun.* **2019**, *5*, 136. [CrossRef]
10. Swain, R.B.; Karimu, A. Renewable electricity and sustainable development goals in the EU. *World Dev.* **2020**, *125*, 104693. [CrossRef]
11. Ojo, E.E.; Zulu, M.L.; Akinrinde, A.O. The Modelling and Simulation Of Power Flow and Fault Analysis For A Hybrid DC Microgrid. In Proceedings of the 2021 IEEE PES/IAS PowerAfrica, Nairobi, Kenya, 23–27 August 2021; IEEE: Washington, DC, USA, 2021; pp. 1–5.
12. Pogaku, N.; Prodanovic, M.; Green, T.C. Modeling, analysis and testing of autonomous operation of an inverter-based microgrid. *IEEE Trans. Power Electron.* **2007**, *22*, 613–625. [CrossRef]
13. Buraimoh, E.; Davidson, I. Investigation of the low voltage ride-through of inverter using virtual inertia methods in microgrid. *Int. J. Eng. Res. Afr.* **2019**, *44*, 200–212. [CrossRef]
14. Buraimoh, E.; Davidson, I.E. Comparative Analysis of the Fault Ride-Through Capabilities of the VSG Methods of Microgrid Inverter Control under Faults. In Proceedings of the 2019 Southern African Universities Power Engineering Conference/Robotics and Mechatronics/Pattern Recognition Association of South Africa (SAUPEC/RobMech/PRASA), Bloemfontein, South Africa, 28–30 January 2019; IEEE: Washington, DC, USA, 2019; pp. 400–405.
15. Diaz, G.; Gonzalez-Moran, C.; Gomez-Aleixandre, J.; Diez, A. Composite loads in stand-alone inverter-based microgrids—Modeling procedure and effects on load margin. *IEEE Trans. Power Syst.* **2009**, *25*, 894–905. [CrossRef]
16. Hao, M.; Zhen, X. A control strategy for voltage source inverter adapted to multi—Mode operation in microgrid. In Proceedings of the 2017 36th Chinese Control Conference (CCC), Dalian, China, 26–28 July 2017; IEEE: Washington, DC, USA, 2017; pp. 9163–9168.

17. Fazendeiro, L.M.; Simões, S.G. Historical variation of IEA energy and CO2 emission projections: Implications for future energy modeling. *Sustainability* **2021**, *13*, 7432. [CrossRef]
18. Rocabert, J.; Luna, A.; Blaabjerg, F.; Rodriguez, P. Control of power converters in AC microgrids. *IEEE Trans. Power Electron.* **2012**, *27*, 4734–4749. [CrossRef]
19. Kaviri, S.M.; Pahlevani, M.; Jain, P.; Bakhshai, A. A review of AC microgrid control methods. In Proceedings of the 2017 IEEE 8th International Symposium on Power Electronics for Distributed Generation Systems (PEDG), Florianopolis, Brazil, 17–20 April 2017; IEEE: Washington, DC, USA, 2017; pp. 1–8.
20. Wu, D.; Tang, F.; Dragicevic, T.; Vasquez, J.C.; Guerrero, J.M. Autonomous active power control for islanded ac microgrids with photovoltaic generation and energy storage system. *IEEE Trans. Energy Convers.* **2014**, *29*, 882–892. [CrossRef]
21. Elrayyah, A.; Sozer, Y.; Elbuluk, M. Microgrid-connected PV-based sources: A novel autonomous control method for maintaining maximum power. *IEEE Ind. Appl. Mag.* **2014**, *21*, 19–29. [CrossRef]
22. Elrayyah, A.; Sozer, Y.; Elbuluk, M.E. Modeling and control design of microgrid-connected PV-based sources. *IEEE J. Emerg. Sel. Top. Power Electron.* **2014**, *2*, 907–919. [CrossRef]
23. Du, W.; Jiang, Q.; Erickson, M.J.; Lasseter, R.H. Voltage-source control of PV inverter in a CERTS microgrid. *IEEE Trans. Power Deliv.* **2014**, *29*, 1726–1734. [CrossRef]
24. Patil, M.; Deshpande, A. Design and simulation of perturb and observe maximum power point tracking using matlab/simulink. In Proceedings of the 2015 International Conference on Industrial Instrumentation and Control (ICIC), Pune, India, 28–30 May 2015; IEEE: Washington, DC, USA, 2015; pp. 1345–1349.
25. Tsai, H.-L.; Tu, C.-S.; Su, Y.-J. Development of generalized photovoltaic model using MATLAB/SIMULINK. In Proceedings of the World Congress on Engineering and Computer Science, San Francisco, CA, USA, 22–24 October 2008; pp. 1–6.
26. Oi, A. Design and Simulation of Photovoltaic Water Pumping System. Ph.D. Thesis, California Polytechnic State University, San Luis Obispo, CA, USA, 2005.
27. Masters, G.M. *Renewable and Efficient Electric Power Systems*; John Wiley & Sons: Hoboken, NJ, USA, 2013.
28. Zhao, J.; Graves, K.; Wang, C.; Liao, G.; Yeh, C.-P. A hybrid electric/hydro storage solution for standalone photovoltaic applications in remote areas. In Proceedings of the 2012 IEEE Power and Energy Society General Meeting, San Diego, CA, USA, 22–26 July 2012; IEEE: Washington, DC, USA, 2012; pp. 1–6.
29. Salimath, G.; Singh, N.K.; Badge, S.S. Coordination and performance analysis of pumped hydro storage system integrated with solar, wind hybrid system. In Proceedings of the 2017 International Conference on Energy, Communication, Data Analytics and Soft Computing (ICECDS), Chennai, India, 1–2 August 2017; IEEE: Washington, DC, USA, 2017; pp. 160–164.
30. Boukhezzar, B.; Lupu, L.; Siguerdidjane, H.; Hand, M. Multivariable control strategy for variable speed, variable pitch wind turbines. *Renew. Energy* **2007**, *32*, 1273–1287. [CrossRef]
31. Chung, I.-Y.; Liu, W.; Cartes, D.A.; Schoder, K. Control parameter optimization for a microgrid system using particle swarm optimization. In Proceedings of the 2008 IEEE International Conference on Sustainable Energy Technologies, Singapore, 24–27 November 2008; IEEE: Washington, DC, USA, 2008; pp. 837–842.
32. Antoniadou-Plytaria, K.E.; Kouveliotis-Lysikatos, I.N.; Georgilakis, P.S.; Hatziargyriou, N.D. Distributed and decentralized voltage control of smart distribution networks: Models, methods, and future research. *IEEE Trans. Smart Grid* **2017**, *8*, 2999–3008. [CrossRef]
33. Sahoo, S.K.; Sinha, A.K.; Kishore, N. Control techniques in AC, DC, and hybrid AC–DC microgrid: A review. *IEEE J. Emerg. Sel. Top. Power Electron.* **2017**, *6*, 738–759. [CrossRef]
34. Bidram, A.; Nasirian, V.; Davoudi, A.; Lewis, F.L. *Cooperative Synchronization in Distributed Microgrid Control*; Springer: Berlin/Heidelberg, Germany, 2017.
35. Russell, S.J. *Artificial Intelligence A Modern Approach*; Pearson Education, Inc.: New York, NY, USA, 2010.
36. Hug, G.; Kar, S.; Wu, C. Consensus+ innovations approach for distributed multiagent coordination in a microgrid. *IEEE Trans. Smart Grid* **2015**, *6*, 1893–1903. [CrossRef]
37. Kouveliotis-Lysikatos, I.N.; Koukoula, D.I.; Hatziargyriou, N.D. A double-layered fully distributed voltage control method for active distribution networks. *IEEE Trans. Smart Grid* **2017**, *10*, 1465–1476. [CrossRef]
38. Guo, F.; Wen, C.; Song, Y.-D. *Distributed Control and Optimization Technologies in Smart Grid Systems*; CRC Press: Boca Raton, FL, USA, 2017.
39. Paquin, J.-N.; Moyen, J.; Dumur, G.; Lapointe, V. Real-time and off-line simulation of a detailed wind farm model connected to a multi-bus network. In Proceedings of the 2007 IEEE Canada Electrical Power Conference, Montreal, QC, Canada, 25–26 October 2007; IEEE: Washington, DC, USA, 2007; pp. 145–152.
40. Golroodbari, S.; Vaartjes, D.; Meit, J.; Van Hoeken, A.; Eberveld, M.; Jonker, H.; Van Sark, W. Pooling the cable: A techno-economic feasibility study of integrating offshore floating photovoltaic solar technology within an offshore wind park. *Sol. Energy* **2021**, *219*, 65–74. [CrossRef]

41. Rahman, A.U.; Syed, I.; Ullah, M. Small-signal stability criteria in AC distribution systems—A review. *Electronics* **2019**, *8*, 216. [CrossRef]
42. Zhang, M.; Han, Y.; Liu, Y.; Zalhaf, A.S.; Zhao, E.; Mahmoud, K.; Darwish, M.M.; Blaabjerg, F. Multi-timescale modeling and dynamic stability analysis for sustainable microgrids: State-of-the-art and perspectives. *Prot. Control Mod. Power Syst.* **2024**, *9*, 1–35. [CrossRef]
43. Gullì, F.; Balbo, A.L. The impact of intermittently renewable energy on Italian wholesale electricity prices: Additional benefits or additional costs? *Energy Policy* **2015**, *83*, 123–137. [CrossRef]
44. De Vries, B.J.; Van Vuuren, D.P.; Hoogwijk, M.M. Renewable energy sources: Their global potential for the first-half of the 21st century at a global level: An integrated approach. *Energy Policy* **2007**, *35*, 2590–2610. [CrossRef]
45. Broughel, A.E.; Hampl, N. Community financing of renewable energy projects in Austria and Switzerland: Profiles of potential investors. *Energy Policy* **2018**, *123*, 722–736. [CrossRef]
46. Guelpa, E.; Bischi, A.; Verda, V.; Chertkov, M.; Lund, H. Towards future infrastructures for sustainable multi-energy systems: A review. *Energy* **2019**, *184*, 2–21. [CrossRef]
47. Jurasz, J.; Canales, F.; Kies, A.; Guezgouz, M.; Beluco, A. A review on the complementarity of renewable energy sources: Concept, metrics, application and future research directions. *Sol. Energy* **2020**, *195*, 703–724. [CrossRef]
48. Yallamilli, R.S.; Vedulla, L.K.; Mishra, M.K. Cost savings oriented microgrid control strategy considering battery degradation. In Proceedings of the 2018 7th International Conference on Renewable Energy Research and Applications (ICRERA), Paris, France, 14–17 October 2018; IEEE: Washington, DC, USA, 2018; pp. 661–666.
49. Goud, S.; Rao, B.L. PV-Wind Integrated Grid with P&O and PSO MPPT Techniques. *Int. J. Recent Technol. Eng. (IJRTE)* **2019**, *8*, 3217–3224.
50. Goud, B.S.; Varma, P.S.; Rao, B.L.; Reddy, M.S.K.; Pandian, A.; Reddy, C.R. Cuckoo search optimization based MPPT for integrated DFIG-wind energy system. In Proceedings of the 2020 International Conference on Decision Aid Sciences and Application (DASA), Sakheer, Bahrain, 8–9 November 2020; IEEE: Washington, DC, USA, 2020; pp. 636–639.
51. Srikanth Goud, B.; Rao, B.L.; Devi, B.N.; Kumar, K.S.; Keerthi, N. Review on optimization techniques employed in distribution generation. *J. Crit. Rev.* **2020**, *7*, 639–645.
52. Uzair, M.; Li, L.; Zhu, J.G.; Eskandari, M. A protection scheme for AC microgrids based on multi-agent system combined with machine learning. In Proceedings of the 2019 29th Australasian Universities Power Engineering Conference (AUPEC), Nadi, Fiji, 26–29 November 2019; IEEE: Washington, DC, USA, 2019; pp. 1–6.
53. Singh, P.; Lather, J.S. Artificial neural network-based dynamic power management of a DC microgrid: A hardware-in-loop real-time verification. *Int. J. Ambient. Energy* **2022**, *43*, 1730–1738. [CrossRef]
54. Shokoohi, S.; Golshannavaz, S.; Khezri, R.; Bevrani, H. Intelligent secondary control in smart microgrids: An on-line approach for islanded operations. *Optim. Eng.* **2018**, *19*, 917–936. [CrossRef]
55. Khooban, M.H.; Gheisarnejad, M. A novel deep reinforcement learning controller based type-II fuzzy system: Frequency regulation in microgrids. *IEEE Trans. Emerg. Top. Comput. Intell.* **2020**, *5*, 689–699. [CrossRef]
56. Vigneysh, T.; Kumarappan, N. Artificial neural network based droop-control technique for accurate power sharing in an islanded microgrid. *Int. J. Comput. Intell. Syst.* **2016**, *9*, 827–838. [CrossRef]
57. Dong, W.Z.; Li, S.H.; Fu, X.G. Artificial neural network control of a standalone DC microgrid. In Proceedings of the 2018 Clemson university power systems conference (PSC), Charleston, SC, USA, 4–7 September 2018; IEEE: Washington, DC, USA, 2018; pp. 1–5.
58. Elsayed, M.; Erol-Kantarci, M.; Kantarci, B.; Wu, L.; Li, J. Low-latency communications for community resilience microgrids: A reinforcement learning approach. *IEEE Trans. Smart Grid* **2019**, *11*, 1091–1099. [CrossRef]
59. Saadatmand, S.; Nia, M.S.S.; Shamsi, P.; Ferdowsi, M. Dual heuristic dynamic programing control of grid-connected synchronverters. In Proceedings of the 2019 North American Power Symposium (NAPS), Wichita, KS, USA, 13–15 October 2019; IEEE: Washington, DC, USA, 2019; pp. 1–6.
60. Kim, H.; Ahmad, A.; Hwang, J.; Baqa, H.; Gall, F.L.; Ortega, M.A.R. IoT-TaaS: Towards a prospective IoT testing framework. *IEEE Access* **2018**, *6*, 15480–15493. [CrossRef]
61. Moayedi, S.; Davoudi, A. Distributed tertiary control of DC microgrid clusters. *IEEE Trans. Power Electron.* **2015**, *31*, 1717–1733. [CrossRef]
62. Shang, L.; Li, P.; Li, Z. Low voltage ride through control method of photovoltaic grid-connected inverter based on model current predictive control. In Proceedings of the 2018 Chinese Control and Decision Conference (CCDC), Shenyang, China, 9–11 June 2018; IEEE: Washington, DC, USA, 2018; pp. 5209–5214.

Disclaimer/Publisher's Note: The statements, opinions and data contained in all publications are solely those of the individual author(s) and contributor(s) and not of MDPI and/or the editor(s). MDPI and/or the editor(s) disclaim responsibility for any injury to people or property resulting from any ideas, methods, instructions or products referred to in the content.